Final Project

Influence of water microfilm on the sliding of water droplet

Author

Ignacio Jaime Domingo

Director

Zbigniew Zapałowicz

Faculty of Mechanical Engineering and Mechatronics

2012

1. Nomenclature

A	Hamaker constant (J)
A_{disp}	dispersion constant (J) $= A/6\pi$
E	energy (J)
e_η	unit vector in direction η
F_{disp}	dispersion force (N)
$\overline{F}_{disp}$	molar dispersion force (N mol^{-1})
f	body force per volume (N m^{-3}), condensation coefficient (–)
f^*	body force per mass (N kg^{-1})
g	gravity (m s^{-2})
H	height (m)
K	curvature (m^{-1})
L	length (m)
M	molar mass (kg kmol^{-1})
N_A	Avogadro number (mol^{-1})
n	mole number (mol)
p	pressure (N m^{-2})
$\dot{q}$	heat flux (W m^{-2})
R	gas constant (J kg^{-1} K^{-1})
R_m	universal gas constant (J mol^{-1} K^{-1})
r	radius, radial co-ordinate (m)
S	entropy (J K^{-1})
$\overline{S}$	molar entropy (J mol^{-1} K^{-1})
T	Temperature (K)
V	volume (m^3)
$\overline{V}$	molar volume (m^3 mol^{-1})
W	work (N)
w	interaction pair potential (J)
ξ	co-ordinate (m)
η	co-ordinate (m)
ρ	density (kg m^{-3})
ρ_1, ρ_2	number density (m^{-3}) of species 1 and 2
μ	chemical potential (J mol^{-1})
σ	surface tension (N m^{-1})
δ	film thickness (m)

Subscripts

ad	adsorption
B	bubble
disp	dispersion
G	gas
hydr	hydrodynamical
L	Liquid
mic	micro-region
Ph	at interface
Ph, L	on liquid side of the interface
Ph, G	on gas side of the interface
SL	interaction of solid with liquid
S, L, G	interaction of solid with gas across liquid
S, Lσ, G	interaction of solid with gas across liquid and σ-phase
S, L, σG	interaction of solid with σ- and gas-phase across liquid
sat	saturation
W	wall
η	in direction η
σ	interface between liquid and gas

2. Aim and introduction

The aim of the project is investigate the phenomena of sliding of single water droplet on the flat surface when the solid body is covered by thin water microfilm.

Based in a theory explanation and in the data of next experiments, the dynamic microscopic advanced angle has to be calculate and estimate with the most precision as it is possible. Then, after comparing with previous data experiments, we have to find which parameters have influence in this phenomena and in that way can change the evolution and the results of this phenomena.

Moreover, the investigation of this phenomena have to be a reference for investigators in the future.

3. Intermolecular Forces in Phase-Change Heat Transfer

3.1 Introduction

Experimental observations and theoretical simulations of the effects of long-range intermolecular forces have demonstrated that the properties of small liquid systems Ž such as an evaporating drop. deviate from those of a bulk liquid. Deviations also occur near the junction of a liquid film with a substrate. Still additional deviations occur as the thickness of a thin liquid film decreases (such as near the ‘‘contact line’’ where the liquid-vapor interface intercepts the ‘‘substrate’’). These regions have received extensive study because of their fundamental importance in nature. Herein, this broad literature is reviewed and connected for the purpose of demonstrating its efficacy in modeling change-of-phase heat transfer (such as boiling, heat pipes, grooved evaporators and condensers, rewetting of heated surfaces, and so on). An evaluation of the literature leads us to the conclusion that it is possible to start with two of the four fundamental forces of nature (gravity and electromagnetic (intermolecular)) and obtain the effects of shape (thickness and curvature), concentration, and temperature on the interfacial heat-transfer co- efficient and stability of a thin liquid film. This basic under- standing has led to important developments in heat-transfer systems.

There is an extremely rich literature concerning equilibrium and no equilibrium curved liquid films. Therefore, judicious choices are made so that a coherent and consistent understanding of the phenomena of particular use to change-of-phase heat transfer can be discussed. For example, although computational molecular dynamics is extremely useful in analyzing the dynamics of molecules in small systems, additional development of this field to emphasize interfacial mass transfer is still needed to have an impact on change-of-phase heat-transfer systems. The gradient theory of fluid microstructures is not covered for the same reason translation of van der Waals, Davis and Scriven (1981), and Evans et al. (1986). Instead, models based on classical interfacial kinetic theory, quasi-thermodynamics, and continuum concepts are used to simulate the area averaged results that are experimentally observed. However, additional simulation at the molecular level will be needed as systems become smaller and optimized. In essence, the literature on the effect of a no uniform thin liquid film with shape dependent properties on phase-change heat transfer is reviewed and

connected. There have been experimental evaluations of the applicability of the Kelvin equation to highly curved interfaces. For example, Fisher and Israelachvili (1981) demonstrated the validity of the Kelvin equation with systems as small as 4 nm. Use of the bulk viscosity in extremely small thicknesses is still open to question. For example, conflicting results have been presented by Klein and Kumacheva (1995) and Knudstrup et al. (1995). Although roughness can have an additional effect in some cases, roughness greater than that at approximately the molecular level is not addressed. Concerns about using continuum models with ultra-thin films are partially alleviated by averaging over a sufficiently large surface area and time so that the theoretical results can be experimentally evaluated for confirmation. Confirmed results can then be used for engineering designs.

Since a liquid is deformable, the shape of a liquid film is a function of the three-dimensional (3-D) intermolecular force field. Therefore, the transport processes in a thin film are a function of the liquid-solid system, temperature, concentration, and the shape which is a measure of the varying internal pressure (intermolecular force) field. The optical measurement of shape gives the otherwise difficult measurement of relative pressure in small systems. Two powerful optical techniques based on reflectivity to measure the change in the thin film profile (intermolecular force profile) with heat transfer are discussed herein: image analyzing interferometer (IAI) (DasGupta et al., 1995) and ellipsometry (Kim and Wayner, 1996). Other optical techniques are discussed by Oron et al. (1997).

As outlined in many recent texts, intermolecular and surfaces forces are the result of the electronic structure of atoms and molecules. At equilibrium, these forces cause the adhesion of one substance to another, the cohesion in bulk liquids, the free energy associated with interfaces, and the liquid-vapour phase distribution in a closed system. An early example of the effect of dielectric properties on change-of-phase heat transfer is given by Wayner (1978). The many no covalent intermolecular interactions can be broadly classified as follows:

1. Electrodynamics Lifshitz-van der Waals (LW) forces (comprising the sum of the London dispersion interaction between two apolar molecules or atoms; the Debye induction interaction and the Keesom orientation interaction).

2. Polar forces (hydro- gen bonding and Lewis acid-base interactions)

3. Purely electrostatic forces. The London dispersion forces are always present and control transport processes in very thin films with apolar systems. These dispersion forces are long-range forces, vary inversely with the film thickness raised to a power, and can be effective over large distances: from approximately 100 nm, at which an extremely small change from the bulk vapor pressure over a thin liquid film occurs, down to interatomic spacing (0.2 nm) where the vapor pressure of an adsorbed monolayer can be extremely small. As described by the adsorption isotherm, the thickness of an adsorbed film is a function of the surrounding vapor pressure and substrate temperature. Herein, completely wetting apolar systems will be used as examples because, with simple systems, the van der Waals intermolecular force field can be easily modeled and experimentally studied. Using the insights thereby gained, these concepts can be extended to include more complicated systems.

For a specific example, we start with the description of a constrained vapor bubble (CVB) heat exchanger with transparent quartz walls which embodies many of the concepts that will be subsequently discussed. The CVB, which is presented in Figure 1 for a no isothermal microgravity environment, has various thin film regions that are of both basic and applied interest. It is formed by underfilling an evacuated small container with liquid. For a completely wetting system at equilibrium, liquid will coat all the walls of the container. For a finite contact angle system, some of the walls can have only an extremely small amount of adsorbed vapor, which changes the substrate properties. Liquid will fill a portion of the corners in both cases. Since the solid walls constrain the shape of the vapor bubble and, therefore, the equilibrium liquid film, the intermolecular force field in the thin liquid film is different from that in a bulk liquid. Both equilibrium, with a uniform temperature field, and no equilibrium $T_2 \geq T_1$ studies have been made using the CVB. Although the thermal conductivity of quartz is small, transparent walls remove the uncertainty concerning liquid

shape and are highly desirable in basic research. When heat is supplied at one end and removed at the other end, the effective thermal conductivity due to the evaporation/condensation process can be orders of magnitude greater than that of copper. Vapor flows to the cold end and liquid flows to the hot end due to the shape-dependent intermolecular force gradient. As presented for a relatively large width (± 3 mm), the cross-sectional area for vapor flow is much larger than that for liquid flow. As a result, the pressure in the vapor space is nearly

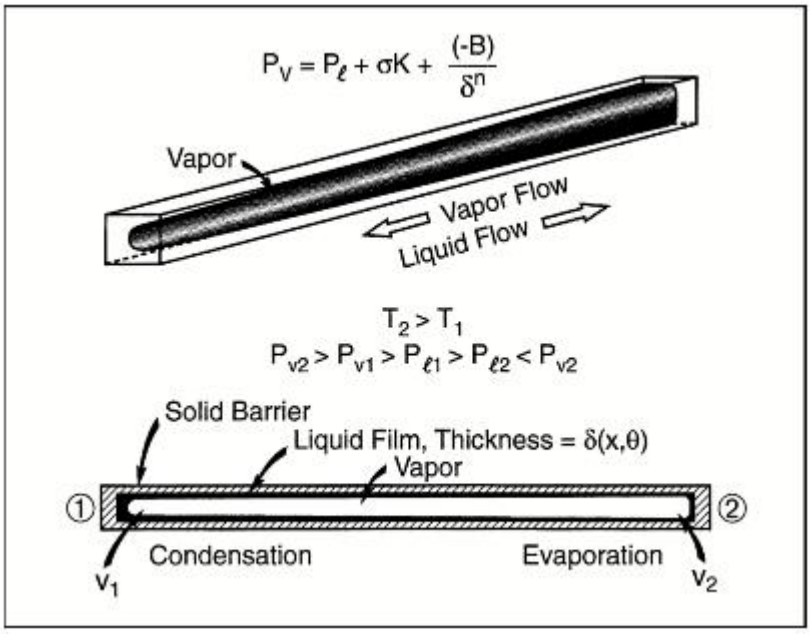

Fig. 1. Constrained vapor bubble concept for a completely wetting system in a microgravity field with heat in at end 2 and heat out at end 1.

constant even with high imposed heat fluxes. In this case, the high interfacial heat-transfer coefficient keeps the liquid-vapor interface nearly isothermal, except where the film is extremely thin. In the ultrathin film region where deviations in the intermolecular force field control the transport processes, large interfacial temperature gradients are sustainable. When sufficiently stressed, dry regions with contact lines occur. At the other extreme, the isothermal system is well suited to the study of interfacial thermodynamics.

3.2 Basic Concepts

3.2.1 Clapeyron effect

Using kinetic theory and the Clausius-Clapeyron equation, an ideal liquid-vapor interfacial heat-transfer coefficient h^{id} can be defined by Eq. 1 as the heat-transfer coefficient associated with the surface of a bulk liquid due to a temperature jump at the liquid-vapor interface. In Eq. 1, T_{lv} is the temperature on the liquid side of a planar liquid-vapor interface and T_v is the temperature on the vapor side.

In Eq. 2, Δh_m is the heat of vaporization and the value of the coefficient can be $C = 2$ for simple systems with an accommodation coefficient of unity. For the reference system, T_v is also the equilibrium temperature of a bulk fluid which has an equilibrium vapor pressure of P_v. This interfacial temperature jump gives a ‘‘ vapor pressure’’ difference for evaporation and vapor flow away from the interface or for condensation with vapor flow towards the interface. As discussed extensively by Carey (1992), extremely high interfacial heat-transfer coefficients are possible.

Additional experimental research on C is reviewed in Maa (1983). Values for the ideal interfacial heat-transfer coefficient for pentane as a function of bulk vapor pressure are given in Figure 4. These large values can be compared with the thermal conductance of the liquid film to determine the thickness at which it becomes important. As an example, for conduction across a liquid pentane film with a thickness of δ=24 nm, $h = k/\delta = 4.8*10^6$ W/m^2 *K. This level was selected, because it is equal to the value of h^{id} at the atmospheric vapor pressure of 10^5 N/m2. We note that significantly larger values of *h*id are attainable with many other systems.

$$q'' = m''^{id}\Delta h_m = h_{lv}^{id}(T_{lv} - T_v) \qquad (1)$$

$$h_{lv}^{id} = \left(\frac{C^2 M}{2\pi R T_{lv}}\right)^{0.5} \frac{M P_v \Delta h_m^2}{R T_v T_{lv}} \qquad (2)$$

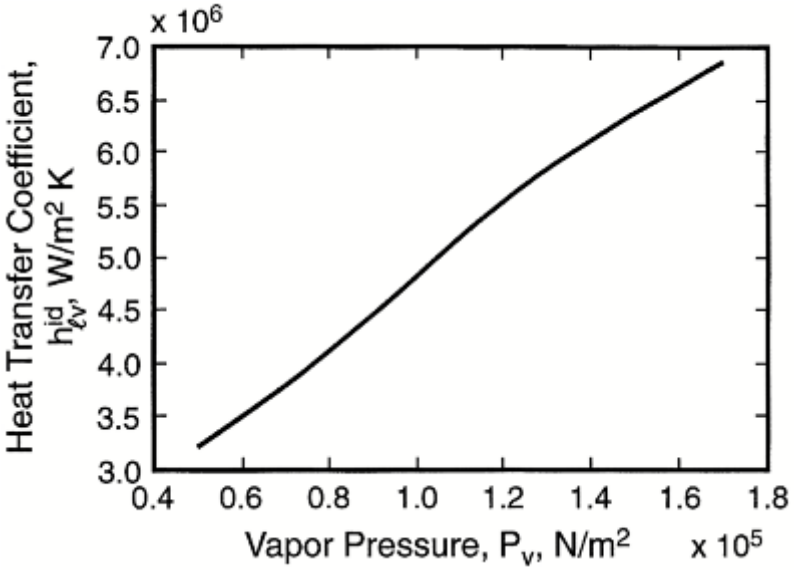

Fig. 4. Ideal value of liquid-vapor interfacial heat-transfer coefficients h_{iv}^{id} for pentane as a function of the vapor pressure of the bulk liquid.

3.2.2 Kelvin effect

Since the values of h^{id}_{iv} and the thermal conductance for thin liquid films are so large, other resistances may limit the heat flux in the contact line region. Three possibilities are the resistance to conduction in the solid, the resistance to fluid flow, and a resistance associated with a change in the vapor pressure of the liquid film due to a change in the intermolecular force field. It is well known that a change in the arrangement of molecules in the interfacial region gives a capillary pressure jump at the interface (such as the interfacial pressure jump associated with the curved meniscus cited above). We find that this shape-dependent change in the intermolecular force field can have a significant, if not controlling, effect on the heat flux in the contact line region.

An example of the variation of chemical potential with film thickness for a thin film is given for a simple spreading case and a simple finite contact angle case in Figure 5a. In the limit $\delta \rightarrow 0$, $\mu \rightarrow -\infty$ for both cases, but this is not shown for $\theta > 0$ due to the extremely small amount of adsorption. The variation for a complicated system which includes a fluid like water on a polar substrate is given in Figure 5b. This represents an adsorbed ultra-thin film in equilibrium with a thicker film at the ‘‘contact line.’’ A discussion of various isotherms is given by Dzyaloskinskii et al. (1961). This early reference is recommended for an understanding of the general theory of van der Waals forces, the DLP thin film continuum model, and the effect of thickness on the vapor pressure.

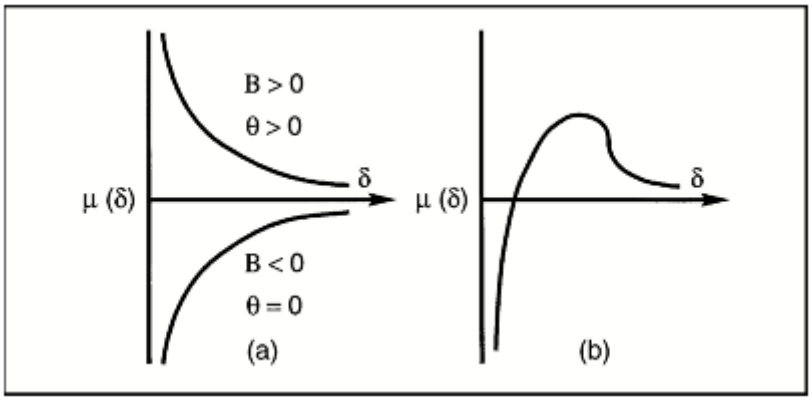

Fig. 5. Variation of chemical potential with film thickness
(a) Simple spreading and nonspreading system
(b) Complicated system (such as water on a polar substrate)

The enhanced Young-Laplace interfacial pressure jump model represented by Eq. 3 which includes both capillary, σK, and disjoining Π pressure jumps, leads to a change in the vapor pressure over the interface relative to that of a planar interface of a bulk liquid. For a completely wetting system, both terms reduce the vapor pressure in the contact line region from that of a bulk liquid. This reduction is given by Eq. 4 in which P_{lv} is the changed vapor pressure of the curved thin film and P_{vr} is the reference vapor pressure. The interface of the bulk fluid is used as an ideal reference where the vapor pressure is the well-known thermodynamic pressure

$$P_v - P_l = \sigma K + \Pi \qquad (3)$$

$$RT_{vr} \ln(P_{lv}/P_{vr}) = -V_{lM}(\Pi + \sigma K) \qquad (4)$$

{Π= - Å / δ^n (for a completely wetting system, Å= A / 6π < 0, where *A* is the fundamental Hamaker constant which is a function of the dielectric properties of the system);
for δ<10 nm, *n*=3 with *A*≈-1.28*10^{-20} J for the pentane/quartz system;
for δ>15 nm, *n*=4, Å=*B* ≈ -1.1* 10^{-29} J*m.

In Figure 6, values for the disjoining pressure jump at the interface of a flat pentane film on quartz are given.

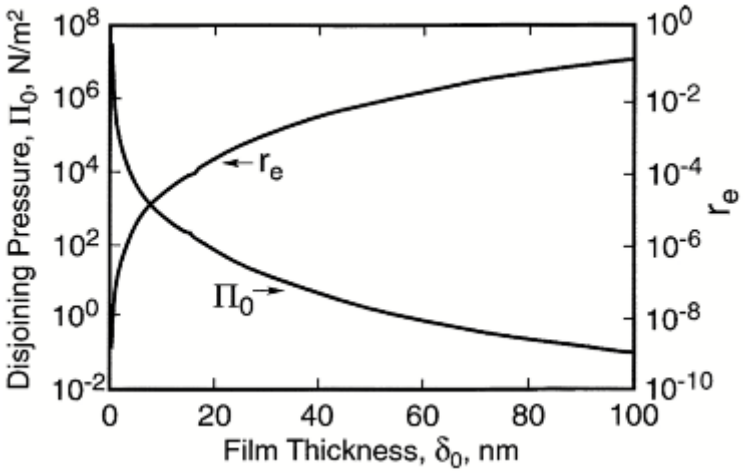

Fig. 6. Equilibrium disjoining pressure

Assuming only capillarity without disjoining pressure for the purpose of discussion, the value of the equivalent radius of curvature for a meniscus is also given for comparison. Large values are obtained as the value of the film thickness approaches that of a monolayer and/or the value of the radius of curvature, r=1/K, becomes very small. We quickly note that both terms should be included in Eq. 3.

A physical understanding of the effect of the interfacial pressure jump on the heat flux can be obtained using the following extended form of Eq. 1, which includes both the Kelvin and Clapeyron effects on the vapor pressure.

$$q'' = m''\Delta h_m = h_{lv}^{\mathrm{id}}(T_{lv} - T_v) + h_{lv}^{kl}(P_l - P_v) \qquad (5)$$

$$h_{lv}^{kl} = \left(\frac{C^2 M}{2\pi R T_{lv}}\right)^{0.5} \frac{V_{lM} P_v \Delta h_m}{R T_{lv}} \qquad (6)$$

For pentane T =293 k, h^{kl}_{iv} = 4.25 (W/m2)/(Nrm2). For a reduction of heat flux of q" = 4.25* 10^6 (W/m2), (P_l - P_v) = -10^6 (N/m2), for which the radius of curvature would have to be equal to r =16 nm. This large effect can be easily present when fluid flows towards the contact line due to intermolecular suction. For an adsorbed flat film with an equivalent disjoining pressure, the equilibrium thickness of the superheated adsorbed film would be δ_o = 0,88 nm.

Therefore, we find that interfacial forces can easily control the heat flux in a superheated adsorbed film. In essence, the Kelvin effect can remove the singularity associated with conduction across a liquid film of vanishing thickness. We also suggest that phase change can remove the singularity usually associated with the "no slip" boundary condition on an "isothermal" or no isothermal substrate in spreading. However, this is usually neglected in current studies on spreading where slip and surface diffusion mechanisms are used to relieve the infinite stress. Although the correct model to use at the contact line is unresolved. It seems that both temperature and pressure should be important.

3.3 Interfacial free energy and Hamaker constant

Equations 3 - 5 demonstrate the importance of surface tension and the Hamaker constant on the interfacial heat-transfer coefficient. To overcome the theoretical difficulties associated with intermolecular forces at interfaces, various useful models have been developed.

Gibbs (1961) developed the very successful surface formalism of a 2-D dividing surface: the Gibbs convention. At times, this convention and the resulting interfacial free energy are extremely useful. In many other situations, like transport processes in ultra-thin liquid films, we find it more useful to include the thickness of the thin film which is not easily described within the Gibbs convention. To include thickness, a 3-D model is needed. This requires either the surface excess convention or the film excess convention. Both the Gibbs and the surface excess conventions are used herein, thereby showing the connection between the two conventions. The surface excess convention allows the disjoining pressure concept, which is an effective pressure change due to intermolecular force changes in a planar thin film, to be introduced.

When a liquid drop is placed on a substrate, the resulting system can be classified as either completely spreading, partially spreading, or no spreading. For complete spreading, the final equilibrium shape is one of a thin uniform film covering the substrate (presuming that the vapor pressure in the surroundings is sufficient to suppress evaporation). Simple diagrams of the completely spreading and partially spreading cases in a gravitational field are presented in Figure 7.

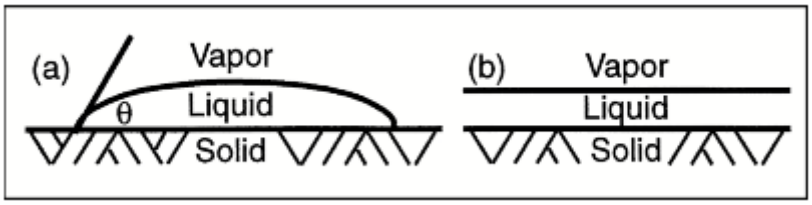

Fig. 7. Simple macroscopic views of a liquid film on a solid substrate (a) Partially wetting liquid droplet; (b) completely wetting liquid film

The picture of the completely wetting case conceptually represents, for an extremely thin case, a monolayer or, at the other extreme, a much thicker film. For the partially wetting case, a deceptively simple quantitative measure of the complex intermolecular force field in the contact line region is the apparent contact angle θ.

The contact angle is defined as the angle between the tangents to the liquid-vapor and liquid-solid interfaces at a point where the film is sufficiently thick so that the transition regions in the interfaces do not overlap. For some cases, like a small drop on a substrate, this definition is still inexact since the observable tangent angle constantly changes. For the nonwetting case, $\theta > 90^o$.

At this point, it is becoming obvious that mathematical interfaces and apparent contact angles are relatively crude but useful (at times) descriptions of the complex dynamic molecular world at interfaces and contact lines. For example, try to picture the real contact angle in the contact line region of a moving contact line using a molecular dynamic simulation model.

The interfacial free energy can be composed of dispersion (London) *d*, polar (Keesom) *p*, induced dipole (Debye) *i*, electrostatic *e*, and acid-base interactions AB.

$$\sigma = \sigma^d + \sigma^p + \sigma^i + \sigma^e + \sigma^{AB} \qquad (7)$$

The first three terms in this equation are the Lifshitz-van der Waals interactions σ^{LW}. Simple fluids like the alkanes have only LW interactions. Some representative values for the terms in Eq. 9 for polar fluids are given by van Oss (1994). For apolar liquids like the alkanes emphasized below, $\sigma = \sigma_l = \sigma^{LW}$.

To connect these concepts and the Hamaker constant with experimental observations, we assume (at times) that there is no practical difference between these processes of interfacial formation occurring in a vacuum and an environment saturated with vapor or gas ($\sigma_l \equiv \sigma_{lv}$, $\sigma_s \equiv \sigma_{sg}$ or σ_{sv}). However it is also important to realize that the interfacial free energy values can, in some cases, be substantially different in laboratory air because of the adsorption of foreign vapor molecules like water and hydrocarbons. At liquid-vapor interfaces, impurities may or may not concentrate at the surface and thereby affect the value of the interfacial free energy.

A further complication can arise if the environment has a foreign gas which can adsorb on the liquid substrate and change σ_l to σ_{lg}. Therefore, there are many practical complications when these concepts are used in modeling transport processes. On the other hand, all these additional effects can be experimentally measured and theoretically modeled. As examples, practical experiments on the effect on the environment on the surface tension of stainless steel are discussed by Mantel and Wightman (1994) and a theoretical analysis of the wetting of gold by water is given by Parsegian (1977). The reader will find it necessary to use, as the situation dictates, both practical and ideal concepts to understand and apply the state of the art in surface transport processes.

The current trend towards smaller closed devices is a trend towards more ideal systems.
Equation 8 is the Young equation for the contact angle of a liquid on a substrate in its equilibrium vapor environment.

$$\sigma_{lv} \cos\theta = \sigma_{sv} - \sigma_{sl} \qquad (8)$$

This can also be written as

$$\sigma_{lv} \cos\theta = \sigma_s - \sigma_{sl} - \pi_e \qquad (9)$$

where $\pi_e = \sigma_s - \sigma_{sv}$ is the equilibrium film pressure which accounts for adsorption on the solid substrate.

4. Influence of dispersion forces on phase equilibria between thin liquid films and their vapour

4.1 Introduction

Micro scale heat and mass transfer in nucleate boiling strongly depends on vapour–liquid phase equilibria of a thin liquid film adsorbed between the heated wall and the vapour bubble as first pointed out by Stephan and Hammer [1]. As an example, in Fig. 1 the curved line represents the interface between a vapour bubble and the liquid layer at a heated wall. In the so-called macro region the interface has an almost constant curvature K corresponding to the bubble radius r_B, $K = 2 / r_B$.

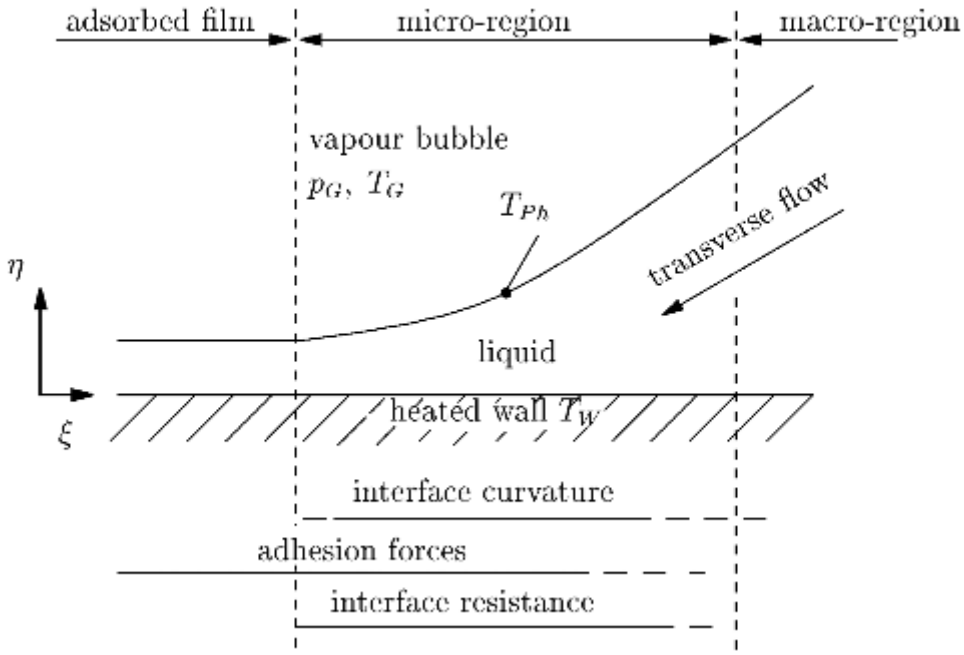

Fig. 1. Liquid film between vapour bubble and heated wall: (—) region of strong influence and (- - -) region of weak influence

In the micro-region the curvature of the interface sharply turns and ends in a non-evaporating liquid film adsorbed at the wall, the curvature being there K = 0. In this adsorbed film, in the so-called adhesion zone between wall and liquid film, attractive forces inhibit evaporation. In the micro-region between macro-region and the adsorbed film the curvature of the liquid–vapour interface undergoes a steep maximum, which for example for refrigerant R114 of 0.247 MPa boiling at a wall super- heated by 5 K, amounts to $K_{max} \approx 10^7$ m^{-1} .

The curvature varies over a small distance of about 0.1 µm between that of the adsorbed film K = 0, the maximum value Kmax ≈ 10^7 m^{-1} in the micro-region and an almost constant value K ≈ 10^3 m^{-1} in the macro-region, thus leading to extremely high capillary forces, a strong liquid flow towards the interface, and hence in the thin liquid film to extreme high heat fluxes of up to 10^7 W/m2 [1–6].

Phase equilibria at the liquid–vapour interface are different from those at plane interfaces free of dispersion forces for three reasons:

1) The capillary forces due to the strong change in curvature in the micro-region also enhance the interface temperature T_{PH}. The superheat over saturation temperature of a plane interface necessary for evaporation of the curved interface increases with capillary pressure.

2) Because of the thin liquid film in the micro-region the temperature drop T_W - T_{Ph} between wall and gas–liquid interface can be as small or even smaller than the temperature drop T_{Ph} - T_G between gas– liquid interface and gas-core. The molecular kinetic resistance at the liquid–vapour interface has to be taken into account.

3) In the adhesion zone and the micro-region long range interaction forces, so called dispersion forces, between solid wall and the molecules of the thin liquid film rise the temperature T_{Ph} at the interface.

Because of the variation of curvature K(ζ) and film thickness δ(ζ) the interface temperature T_{PH} is not constant but a function of the radial co-ordinate ζ. We can therefore state, as shown in Fig. 2, that the temperature drop T_{Ph} - Tsat is considerable, and thus the driving temperature difference T_W - T_{Ph} for heat transfer is smaller than T_W - Tsat of a plane film, when the dispersion forces and intermolecular resistance are negligible.

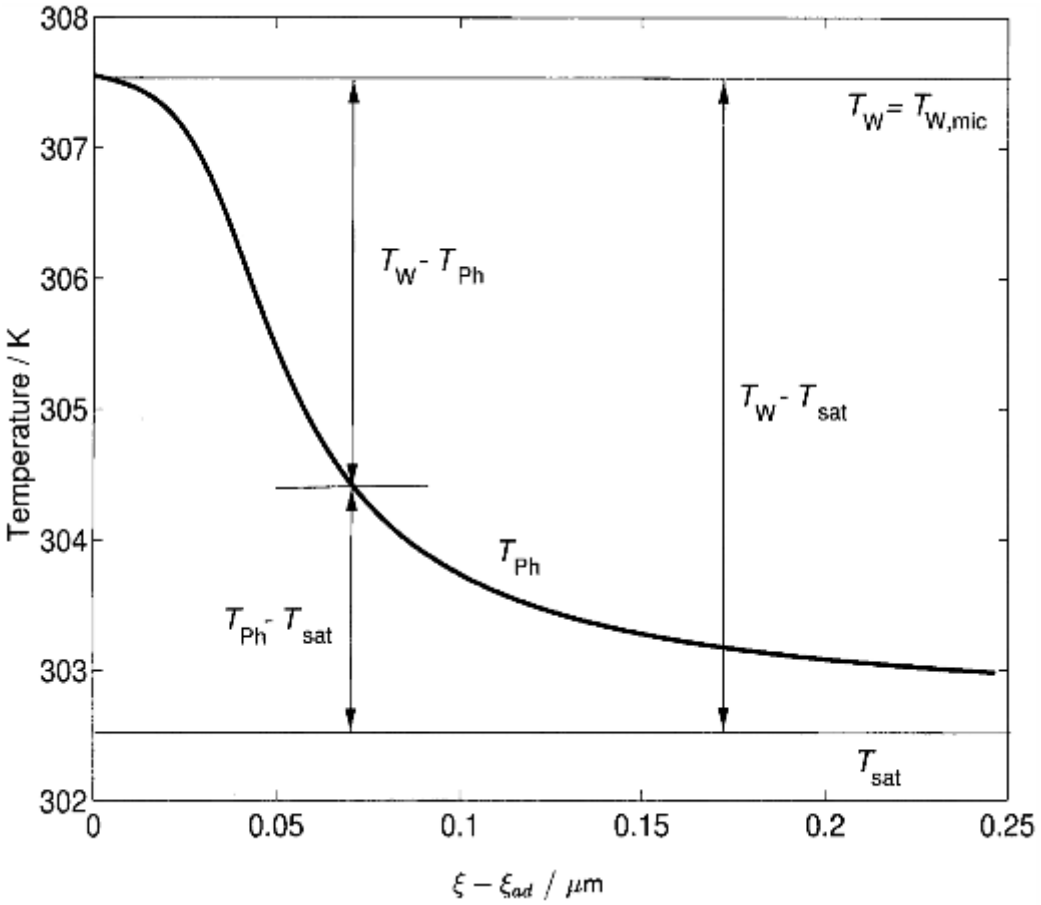

The smaller temperature difference T_W - T_{Ph} compared to T_W - Tsat reduces the heat flux. This reduction in the micro-region, however, is partly compensated by the much smaller thermal resistance of the thin liquid film. Basic and pioneering theoretical and experimental studies of evaporating thin liquid films were mainly performed by Wayner and coworkers.

A concise review of their research is given by Wayner. As shown by them the assumption of a constant interface temperature T_{Ph} and also a constant curvature K = const in the micro-region does not hold.

It is obvious that the liquid–vapour phase change is of fundamental interest and of practical significance in nucleate boiling heat transfer.

A useful tool for the study of phase equilibria is the Kelvin equation, which shall be presented here for pure substances. Its derivation is usually based on the assumption of a fluid with ideal vapour and an incompressible liquid phase. Intermolecular forces between solid and liquid are not taken into account. In our case we also assume an ideal vapour and an incompressible liquid. However, because of the presence of dispersion forces the intermolecular forces between solid and liquid must be taken into account.

They add to the capillary forces. Furthermore the temperature rises at the liquid–vapour interface because of the molecular kinetic resistance. Both effects cause a shift in the chemical potential, which shall be discussed in this paper.

Then, with the aid of the Kelvin equation, deduced from the chemical potential, the variation of pressures in the liquid and vapour phase, as they occur in nucleate boiling when vapour bubbles exist at solid walls, will be studied.

4.2 The nature of dispersion forces

The adhesion of dispersion forces between the solid wall and the liquid film can be attractive or repulsive. As long range forces they can be effective from distances of interatomic spacing in the liquid film of about 0.2 nm to distances of some 10 nm. They are quantum mechanical in origin, and are present even if molecules are non-polar. Though the time average dipole of these molecules vanishes there exists a finite dipole moment given by the instantaneous position of the electron around the protons.

These instantaneous dipoles generate an electric field inducing a dipole moment in any nearly neutral atoms giving rise to an instantaneous attractive force between the atoms. The time average of this force is finite. Attractive forces mainly determine the boiling point and the heat of vaporization of a substance, hence their importance when studying boiling processes.

Dispersion forces were intensively studied by Israelachvili and in earlier papers by Derjaguin, who developed a model to convert these forces into a liquid pressure. The dispersion forces lead to an additional pressure p_{disp} in the liquid film, which under the assumption of an interaction pair potential $w = -C / r^n$ with coefficient C describing the interaction between two molecules and for example n = 6 for van der Waals forces becomes

$$p_{\mathrm{disp}} = A_{\mathrm{disp}}/\eta^3, \qquad (1)$$

where η is the distance between a certain position within the liquid and an infinitely extended solid surface. The dispersion constant describing the interaction between two bodies 1 and 2 is defined as

$$A_{\mathrm{disp}} = \pi C \rho_1 \rho_2 / 6. \qquad (2)$$

ρ1 and ρ2 are the number densities of molecules in the interacting bodies, and coefficient C describes the interaction between the atoms in the bodies. Instead of the dispersion constant A_{disp} the Hamaker constant A, after Hamaker , who did earlier studies to explore the forces between macroscopic bodies, is often used in the literature,

$$A = 6\pi A_{\mathrm{disp}}. \qquad (3)$$

Hamaker constants of van der Waals forces and hence dispersion constants can be calculated from bulk properties such as dielectric constants and refractive indices.

4.3 The chemical potential of system dispersion forces

With the aid of dispersion forces we can now proceed to determine the chemical potential of a homogeneous bulk phase, for instance the liquid phase in Fig. 3.

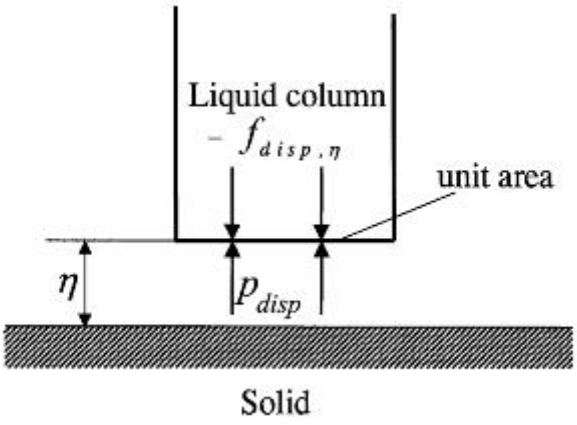

Fig. 3. Dispersion forces acting on a liquid volume of unit area

In all the literature known to the author, it is taken from the Gibbs–Duhem equation

$$d\mu = -\bar{S}\,dT + \bar{V}\,dp, \quad \text{or from}$$
$$d\mu = -\bar{S}\,dT + \bar{V}\,dp + M\vec{g}\,dr$$

if gravity is not negligible. Quantities with an overbar represent molar quantities: S(*p, T*) are the molar entropy and V(*p, T*) the molar volume. If the above equations for the chemical potential were correct then according to the thermal equation of state V(*p, T*) or p = p(*ρ, T*) where ρ is the density, for an incompressible fluid the pressure inside the fluid would only be a function of temperature.

This is correct when dispersion forces are absent, but does not hold when they are not negligible.

As we saw before, Eq. (1) then the dispersion pressure becomes important, depending on the distance between fluid and the solid surface. We should therefore expect p = p(*ρ, T,r*), where *r* stands for the distance, and hence a chemical potential μ = μ(*ρ, T ,r*) and not μ = μ(*ρ, T*) as in the above equation.

In order to derive the correct chemical potential of liquid phase we start from the Gibbs function

$$E = E(S, V, \vec{r}, n) \qquad (4)$$

with entropy S, volume V, co-ordinate r in the liquid and the mole number n. From Eq. (4) we obtain

$$\mathrm{d}E = T\,\mathrm{d}S - p\,\mathrm{d}V - \vec{F}_{\mathrm{disp}}\mathrm{d}\vec{r} + \mu\,\mathrm{d}n \qquad (5)$$

with

$$\vec{F}_{\mathrm{disp}} := -(\partial E/\partial \vec{r})_{\mathrm{S,V,n}} = \vec{F}_{\mathrm{disp}}(S, V, \vec{r}, n).$$

Temperature T, pressure p, and chemical potential μ are defined as partial derivatives of E, T = δE / δS, p = -δE / δV, μ = δE / δn, but now depend on S, V, r, n.

Strictly speaking, F_{disp} stands here for all forces acting on the system. For reasons of simplicity we disregard all other forces except for the dispersion forces as the most important forces for evaporation of thin liquid films.

Because the Gibbs function E, Eq. (4), is a homogeneous function of first order in the variables S, V, n its Euler-equation reads

$$E = TS - pV + \mu n. \qquad (6)$$

From this we have

$$\mathrm{d}E = T\,\mathrm{d}S + S\,\mathrm{d}T - p\,\mathrm{d}V - V\,\mathrm{d}p + \mu\,\mathrm{d}n + n\,\mathrm{d}\mu.$$

Together with Eq. (5) we obtain the Gibbs-Duhem equation

$$S\,\mathrm{d}T - V\,\mathrm{d}p + \vec{F}_{\mathrm{disp}}\mathrm{d}\vec{r} + n\,\mathrm{d}\mu = 0. \qquad (7)$$

The chemical potential μ = μ(ρ, T ,r) of the pure liquid therefore is given by

$$\mathrm{d}\mu = -\overline{S}\,\mathrm{d}T + \overline{V}\,\mathrm{d}p - \overline{\vec{F}}_{\mathrm{disp}}\mathrm{d}\vec{r}, \qquad (8)$$

where S, V and F_{disp} again represent molar quantities.

4.4 Dispersion forces and phase equilibria

Different from the chemical potential $d\mu = -S\,dT + V$ in the absence of dispersion forces, Eq. (8) contains the term $F_{disp}\,dr$ of the molar dispersion force $F_{disp.}$ Its quantity can be derived from the interaction energy of dispersion. In the case of two planar surfaces at a distance $r = \eta e_\eta$ apart, one of unit area and infinite depth, for example a liquid and the other infinitely large, for example a solid wall, we have, as shown by Israelachvili, the dispersion energy,

$$W(\eta) = -\pi C \rho_1 \rho_2 / 12\eta^2, \qquad (9)$$

where C comes from the interaction pair potential $w = -C / r^n$ with n = 6, and ρ1 , ρ2 again are the number densities of solid and liquid. The dispersion force $f_{disp,n}$ per unit surface is given by

$$f_{disp,\eta}(\eta) = -\frac{\partial W}{\partial \eta} = -\pi C \rho_1 \rho_2 / 6\eta^3 = -A_{disp}/\eta^3. \qquad (10)$$

The dispersion force $f_{disp,n}(\eta)$ between two bodies, for example a solid wall and a liquid, as shown in Fig. 3 is the resultant of all body forces due to dispersion acting on the liquid column and directed against the co- ordinate g. Because of the equilibrium of all forces acting on the liquid column at rest the force $f_{disp,n}$ is balanced by an external pressure, the so-called dispersion pressure defined as

$$p_{disp} := -f_{disp,\eta} = A_{disp}/\eta^3. \qquad (11)$$

The dispersion pressure acts in a similar way as the hydrostatic pressure p_{hydr}. Both pressures balance out body forces, the dispersion pressure those of molecular origin, the hydrostatic pressure those of gravity.

However, different from the hydrostatic pressure which decreases linearly with height g according to $\delta p_{hydr} / \delta\eta = -\rho_L g$, the dispersion pressure decreases much faster with $1/\eta^3$ as can be seen from Eq. (11), and we have $\delta p_{disp} / \delta\eta = -\pi C \rho_1 \rho_2 / 2\eta^4$. The dispersion pressure tends to zero mostly after distances η above 100 nm, depending on the substances involved.

We consider now the momentum balance of a fluid volume element dV = *A*dη, where *A* is the surface area, replacing the unit area of Fig. 3. The momentum balance reads

$$\rho_{\mathrm{L}} f^{*}_{\mathrm{disp},\eta} = \frac{\partial p_{\mathrm{disp}}}{\partial \eta}, \qquad (12)$$

where $f^{*}_{\mathrm{disp,n}}$ stands for the body force per mass (SI-unit N / kg) acting on the volume element. Because of

$$\int_V \rho_{\mathrm{L}} f^{*}_{\mathrm{disp},\eta}\,\mathrm{d}\eta = \int_V (\partial p_{\mathrm{disp}}/\partial \eta)\,\mathrm{d}\eta = \int_A p_{\mathrm{disp}}\,\mathrm{d}A$$

in the limit V → 0 the volume integral disappears much faster than the surface integral, we have in any cross section $\int_A p\mathrm{disp}\,\mathrm{dA} = 0$. Dispersion forces in any cross section are opposed to each other and cancel. They behave in the same way as hydrostatic forces which also cancel over a surface.

With Eq. (11) we obtain

$$f^{*}_{\mathrm{disp},\eta} = v_{\mathrm{L}} \frac{\partial p_{\mathrm{disp}}}{\partial \eta} = -v_{\mathrm{L}} \frac{3A_{\mathrm{disp}}}{\eta^4}. \qquad (13)$$

The molar body force F_{disp} (SI-unit N / mol) is

$$\overline{F}_{\mathrm{disp},\eta} = \overline{V}_{\mathrm{L}} \frac{\partial p_{\mathrm{disp}}}{\partial \eta} = -\overline{V}_{\mathrm{L}} \frac{3A_{\mathrm{disp}}}{\eta^4}. \qquad (14)$$

From this we obtain

$$\overline{F}_{\mathrm{disp},\eta}\,\mathrm{d}\eta = \overline{V}_{\mathrm{L}} \frac{\partial p_{\mathrm{disp}}}{\partial \eta}\,\mathrm{d}\eta = \overline{V}_{\mathrm{L}}\mathrm{d}p_{\mathrm{disp}}. \qquad (15)$$

Keeping in mind that $A_{disp} = \pi C \rho_1 \rho_2 / 6$ contains in the case of a liquid–solid interaction the liquid number density $\rho_l = \rho_L \equiv dN_L / dV_L = N_A dn_L / dV_L = N_A / V_L$ with the Avogadro number N_A and the solid number density ρ2 the molar body force can be rewritten

$$\overline{F}_{\mathrm{disp},\eta} = -\frac{\pi C N_A \rho_2}{2\eta^4}. \qquad (16)$$

If gravity plays a role in addition to the dispersion forces the momentum balance becomes $\rho_L f_\eta = \rho_L (f_{g,\eta} + f^*_{disp,n}) = \delta p_L / \delta \eta$ with gravity $f_{g,\eta} = -g$ and $f^*_{disp,n}$ from Eq. (13).

In the liquid film $0 \leq \eta \leq \delta$ gravity is however mostly negligible as we can see from the ratio of dispersion forces and gravity

$$\frac{f^*_{\mathrm{disp},\eta}}{f_{g,\eta}} = \frac{v_L \pi C \rho_1 \rho_2}{2\eta^4 g} = \frac{3A_{\mathrm{disp}}}{\eta^4 \rho_L g} \geqslant \frac{3A_{\mathrm{disp}}}{\delta^4 \rho_L g} \cong 3.6 \times 10^7.$$

As an example we used herein the values $A_{disp} = 8.69 * 10^{-21}$ J for solid-liquid interaction, $\rho_L = 1441$ kg/m^3, film thickness $\eta = \delta = 15$ nm for refrigerant R114 at saturation pressure of 0.247 MPa corresponding to a saturation temperature of 302.63 K.

4.4.1 The Young - Laplace equation

The assumptions made in our model are

- The gaseous phase obeys the equation of state of an ideal gas. Then interactions between gas - molecules disappear.

- The system studied here consists of a solid wall wetted by an extremely thin liquid film in equilibrium whit its vapour phase. Because of the thin liquid film we can not a priori accept the Gibbs assumption according to which the interlayer between gas and liquid is a geometrical surface. Its thickness can be of the same order as that of the liquid film.

Molecular dynamics simulation of the liquid - vapour interface of a Lennard-Jones fluid with real gaseous phases has indeed shown that the thickness of the interlayer is of the order of a few Nanometers.

When the gaseous phase may be considered as ideal the interfacial thickness comes close to 1 nm. Of the same order of magnitude are liquid films in the micro-region, so that the Gibbs-assumption according to which the thickness of the interlayer is negligible compared to that of the liquid film, at least in some parts of the micro-region does not hold.

In order to derive the Young–Laplace equation describing the mechanical equilibrium in such a system we consider, as shown in Fig. 4a, two homogeneous bulk phases consisting of liquid L and gas G, connected by an interface layer σ, having for the sake of simplicity the form of a circular cylindrical shell element of arc length $r\mathrm{d}\theta$, depth L and of thickness Δr. Then the forces σL exerted by surface tension σ act upon the side edges of depth L.

Their resultant is given by $\mathrm{d}F_R = \sigma L \mathrm{d}\varphi$. Also of importance are the forces resulting from gas and liquid pressures and from dispersion. The force balance is given by

$$p_L \cdot (r + \Delta r) \cdot \mathrm{d}\varphi L + \mathrm{d}F_R = p_G r \,\mathrm{d}\varphi L + \mathrm{d}F_{disp}. \qquad (17)$$

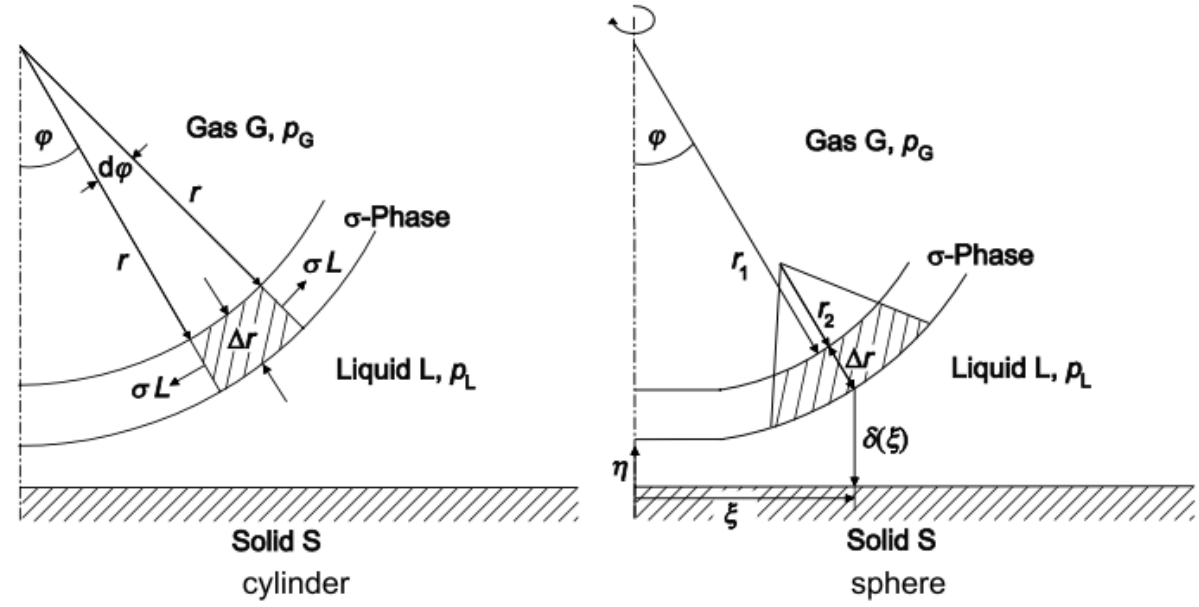

Fig. 4. Mechanical equilibrium between liquid L, gas G and σ-phase: (a) cylinder and (b) main curvatures r_1, r_2

The dispersion forces act as body forces upon the cylindrical shell, and are equal to the difference of the dispersion pressure forces on both sides of the interface.

$$\mathrm{d}F_{\mathrm{disp}} = (p_{\mathrm{disp,Ph,L}} - p_{\mathrm{disp,Ph,G}})r\,\mathrm{d}\varphi L$$

With this the force balance reads

$$p_{\mathrm{L}} \cdot (r + \Delta r) \cdot \mathrm{d}\varphi L + \sigma\,\mathrm{d}\varphi L = p_{\mathrm{G}} r\,\mathrm{d}\varphi L + (p_{\mathrm{disp,Ph,L}} - p_{\mathrm{disp,Ph,G}})r\,\mathrm{d}\varphi L,$$

or because of $\Delta r << r$,

$$p_{\mathrm{L}} + \frac{\sigma}{r} = p_{\mathrm{G}} + p_{\mathrm{disp,Ph,L}} - p_{\mathrm{disp,Ph,G}}. \qquad (18)$$

For a surface with mean curvature $K = 1/r_1 + 1/r_2$, as shown in Fig. 4b, the equivalent balance reads

$$p_{\mathrm{L}} + \sigma K = p_{\mathrm{G}} + p_{\mathrm{disp,Ph,L}} - p_{\mathrm{disp,Ph,G}}. \qquad (19)$$

This is the Young–Laplace equation for a system with dispersion forces. For a Gibbs interface, because of $\Delta r = 0$ and hence $p_{disp,Ph,L} = p_{dispPh,G}$ converts into the well known form of the Young–Laplace equation for a system without dispersion forces $p_L + \sigma K = p_G$.

It is noteworthy that in all references known to the author Eq. (19) is pretended to write

$$p_L + \sigma K = p_G - p_{disp}.$$

Different from Eq. (19) the dispersion pressure does not disappear at a Gibbs interface.
In Eq. (19) the location of $p_{disp,Ph,L}$ in cylinder coordinates is at position φ, $r_1 + \Delta r$ or in Cartesian coordinates at ξ, δ (see Fig. 4b). The cylinder co-ordinates of $p_{disp,Ph,L}$ are φ, r_1 and its Cartesian co-ordinates $\xi - \Delta r_1 \sin\varphi$, $\delta + \Delta r \cos\varphi$. With this the dispersion pressures in the Cartesian co-ordinate system are

$$p_{disp,Ph,L} = A_{disp,Ph,L}/\delta^3 \quad \text{and} \quad p_{disp,Ph,G} = A_{disp,Ph,G}/(\delta + \Delta r\cos\varphi)^3. \qquad (20)$$

The dispersion force leading to the pressure $p_{disp,Ph,L}$ is caused by the interaction of the solid wall S with the σ and the gas-phase G across the liquid film L. Following the notation of Israelachvili the corresponding dispersion constant for the interaction can be written $A_{disp,Ph,L} = A_{S,L,\sigma G} / 6\pi$.

For the interaction of the solid wall S with the gas G across the liquid L and the σ-phase we have $A_{disp,Ph,G} = A_{S,L\sigma,G} / 6\pi$. Approximate combining rules for the Hamaker constants were given for example by Israelachvili and can be written in the following form

$$A_{disp,Ph,L}6\pi = A_{S,L,\sigma G} \approx \left(\sqrt{A_{SS}} - \sqrt{A_{LL}}\right)\left(\sqrt{A_{\sigma G,\sigma G}} - \sqrt{A_{LL}}\right) \qquad (21)$$

and

$$A_{\text{disp,Ph,G}}6\pi = A_{\text{S,L}\sigma\text{,G}} \approx \left(\sqrt{A_{\text{SS}}} - \sqrt{A_{\text{L}\sigma\text{,L}\sigma}}\right)\left(\sqrt{A_{\text{GG}}} - \sqrt{A_{\text{L}\sigma\text{,L}\sigma}}\right). \quad (22)$$

Herein the Hamaker constants A_{ii} are those of two dielectric or electrically non-conducting media i interacting across vacuum. They are given by the Lifshitz theory

$$A_{ii} = \frac{3}{4}kT\left(\frac{\varepsilon_i - 1}{\varepsilon_i + 1}\right)^2 + \frac{3h\nu_e}{16\sqrt{2}}\frac{(n_i^2 - 1)^2}{(n_i^2 + 1)^{3/2}}, \quad (23)$$

where ε_i is the dielectric constant of medium i, n_i its refractive index in the visible, k is the Boltzmann constant, h the Planck constant and ν_e the Plasma frequency of the free electron.

In nucleate boiling processes the solid wall is mostly a metal. For two metals interacting across vacuum the Hamaker constant is $A_{SS} \approx 4*10^{-19}$ J. The Hamaker constants $A_{S,L,\sigma G}$ and $A_{S,L\sigma,G}$ are both negative, because of $A_{SS} > A_{L\sigma,L\sigma} > A_{LL,}$ $A_{LL} > A_{\sigma G,\sigma G}$ and $A_{GG} = 0$.

The negative sign is in agreement with the usually adopted sign convention according to which attractive forces are negative and repulsive forces positive.

As follows then from the definition Eq. (11), dispersion pressures due to attractive forces are positive and those due to repulsive forces negative. The interaction forces between a solid wall and a wetting liquid surpass those between solid wall and gas- or σ-phase. The gas and σ-phase are kept away from the solid wall through the liquid, an effect which is reflected in negative values of the Hamaker constants $A_{S,L,\sigma G}$ and $A_{S,L\sigma,G.}$

4.4.2 The Kelvin equation

With Eq. (15) the chemical potential Eq. (8) of a system with dispersion forces can be written

$$\mathrm{d}\mu = -\overline{S}\,\mathrm{d}T + \overline{V}\,\mathrm{d}p - \overline{V}\,\mathrm{d}p_{\mathrm{disp}}. \qquad (24)$$

Hence the chemical potential is $\mu = \mu(T,p,p_{disp})$. Strictly speaking a gravity term Mgdr should also appear in Eq. (24). As we are interested in phase equilibria this term appears, however, in the chemical potential of all phases in equilibrium and therefore cancels. We can leave it out here.

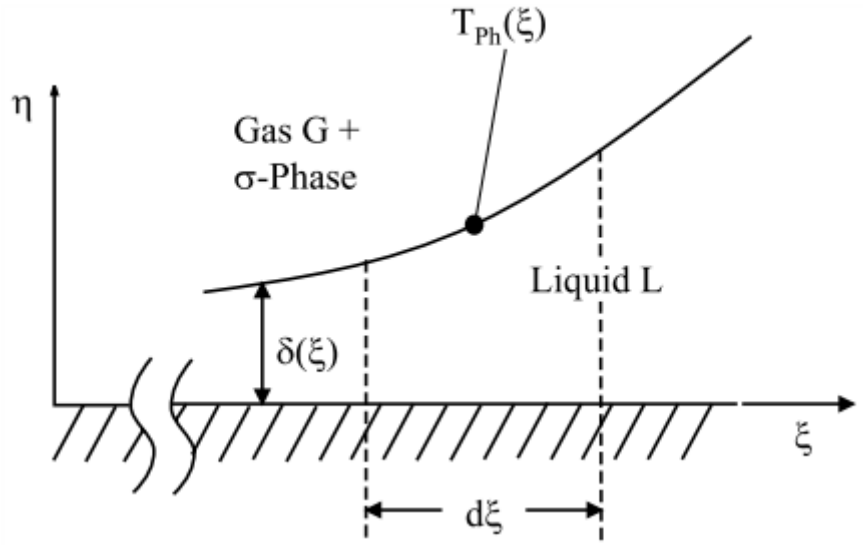

Fig. 5. Local phase equilibrium between liquid L with gas G and σ-phase.

We consider now (Fig. 5) an element dξ of a curved liquid film L of thickness δ(ξ) in phase equilibrium with its vapour G and the σ-phase between liquid and vapour. The temperature at the interfaces and in the σ-phase be $T_{Ph}(\xi)$, the liquid-side pressure $p_{Ph,L}$ and the gas-side pressure $p_{Ph,G}$. Phase equilibrium requires

$$\mu_{\mathrm{L}}(T_{\mathrm{Ph}}, p_{\mathrm{Ph,L}}, \eta = \delta) = \mu_{\mathrm{G}}(T_{\mathrm{Ph}}, p_{\mathrm{Ph,G}}, \eta = \delta + \Delta r \cos\varphi). \qquad (25)$$

The condition for phase equilibrium at temperature T_{Ph} of the same substance if it had a plane interface and if dispersion forces were negligible would be

$$\mu_L(T_{Ph}, p_{sat}, \eta \to \infty) = \mu_G(T_{Ph}, p_{sat}, \eta \to \infty). \qquad (26)$$

From that follows $p_{sat} = p_{sat}(T_{Ph})$. From Eqs. (25) and (26) we obtain

$$\begin{aligned}\mu_L(T_{Ph}, p_{Ph,L}, \eta = \delta) - \mu_L(T_{Ph}, p_{sat}, \eta \to \infty) \\ = \mu_G(T_{Ph}, p_{Ph,G}, \eta = \delta + \Delta r \cos\varphi) \\ - \mu_G(T_{Ph}, p_{sat}, \eta \to \infty)\end{aligned}$$

and hence from Eq. (24) for a given interface temperature T_{Ph}:

$$\begin{aligned}\int_{p_{sat}}^{p_{Ph,L}} \overline{V}_L \, dp - \int_{\eta\to\infty}^{\delta} \overline{V}_L \, dp_{disp} \\ = \int_{p_{sat}}^{p_{Ph,G}} \overline{V}_G \, dp - \int_{\eta\to\infty}^{\delta+\Delta r\cos\varphi} \overline{V}_G \, dp_{disp}.\end{aligned}$$

Assuming the liquid and the gas to be incompressible, we obtain

$$\begin{aligned}\overline{V}_L(p_{Ph,L} - p_{sat}) - \overline{V}_L p_{disp,Ph,L} \\ = \overline{V}_G(p_{Ph,G} - p_{sat}) - \overline{V}_G p_{disp,Ph,G}. \qquad (27)\end{aligned}$$

The pressures $p_{Ph,L}$ at the liquid interface and $p_{Ph,G}$ at the vapour interface are connected by Eq. (19), in which the interface pressures $p_{Ph,L}$ and $p_{Ph,G}$ now replace the pressures p_L and p_G of the homogeneous phases. Elimination of p $p_{Ph,L}$ in Eq. (27) and introducing the density ρ instead of the molar volume V = M / ρ with molar mass M, we obtain the Kelvin equation for the gas-side pressure

$$p_{Ph,G} = p_{sat}(T_{Ph}) - \frac{\rho_G}{\rho_L - \rho_G}\sigma K + p_{disp,Ph,G}. \qquad (28)$$

Corresponding, elimination of $p_{Ph,G}$ in Eq. (27) yields the kelvin equation for the liquid-side pressure

$$p_{\mathrm{Ph,L}} = p_{\mathrm{sat}}(T_{\mathrm{Ph}}) - \frac{\rho_{\mathrm{L}}}{\rho_{\mathrm{L}} - \rho_{\mathrm{G}}}\sigma K + p_{\mathrm{disp,Ph,L}}. \qquad (29)$$

It should be noted that the dispersion pressures $p_{disp,Ph,G}$ and $p_{disp,Ph,L}$ on both sides of the σ-interface are negative for a wetting liquid, as stated before.

The Kelvin equations, Eqs. (28) and (29), hold for local equilibrium of any evaporating system independently if it is open or closed. For a spherical bubble (closed system) of constant curvature K in a liquid faroff from the solid wall we obtain the well known relations

$$p_{\mathrm{Ph,G}} = p_{\mathrm{sat}}(T_{\mathrm{Ph}}) - \frac{\rho_{\mathrm{G}}}{\rho_{\mathrm{L}} - \rho_{\mathrm{G}}}\sigma K \qquad (30)$$

and

$$p_{\mathrm{Ph,L}} = p_{\mathrm{sat}}(T_{\mathrm{Ph}}) - \frac{\rho_{\mathrm{L}}}{\rho_{\mathrm{L}} - \rho_{\mathrm{G}}}\sigma K. \qquad (31)$$

The liquid pressure $p_{Ph,L}$ and the gas pressure $p_{Ph,G}$ at the temperature T_{Ph} are lower than the saturation pressure T_{sat} (T_{Ph}), Fig. 6. For a given saturation temperature T_{sat} the liquid must be superheated by $\Delta T = T_{Ph} - T_{sat}$ for vapour bubbles to exist.

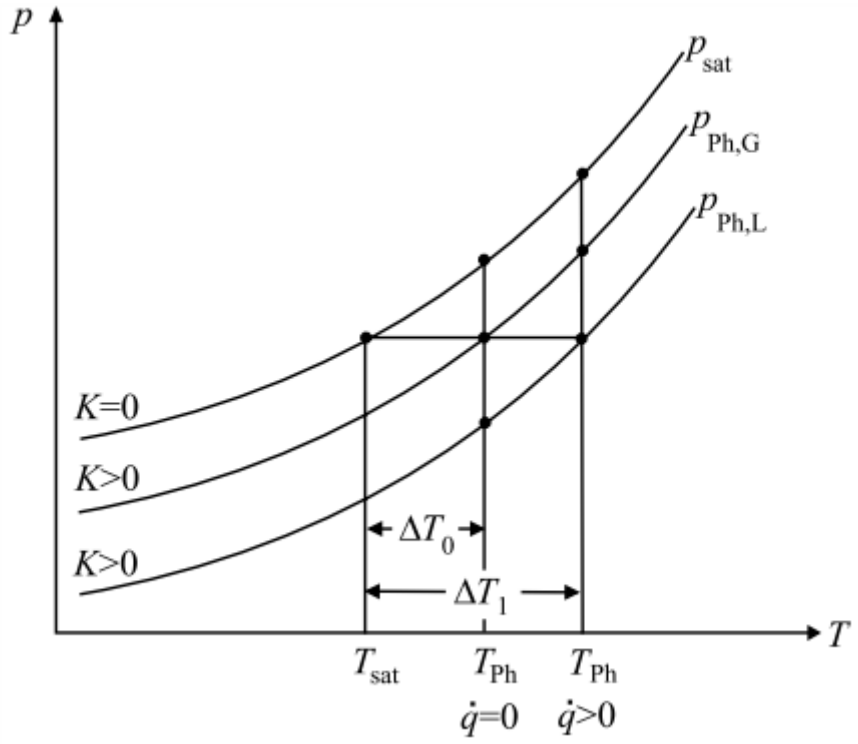

Fig. 6. Liquid and vapour pressure for spherical bubble, curvature K.

4.5 Gas and liquid pressures apart from the interfaces

If evaporation occurs, the gas pressure p_G and the liquid pressure p_L apart from the curved interface δ, Fig.1, differ from the interface pressures $p_{Ph,L}$ and $p_{Ph,G}$. In the bulk of the gas, because of the intermolecular forces, the gas pressure p_G is slightly lower than the interfacial pressure $p_{Ph,G}$, the difference $p_{Ph,G}$ - p_G being the driving force for evaporation. As follows from the kinetic theory or gases we have:

$$p_{Ph,G} - p_G = \dot{q}\frac{2-f}{2f}\frac{[2\pi R T_{sat}(p_G)]^{1/2}}{\Delta h_V}, \qquad (32)$$

with the heat flux q the condensation coefficient f and the enthalpy of evaporation Δh_v. Only for vanishing heat fluxes $q = 0$, we have $p_{Ph,G} = p_G$. In the micro region, where heat fluxes are very high and of the order 10^7 W/m^2 the pressure difference $p_{Ph,G}$ - p_G is not negligible as the following example.

With the aid of the Kelvin equation (28), together with Eq. (24) we also obtain the pressure $p_L(\xi, \eta)$ in the liquid film. Proceeding from the interface $\eta = \delta(\xi)$ where we have $p_{Ph,L} = p_{Ph,L}(\xi, \eta = \delta)$ in the direction η and neglecting gravity in the very thin liquid film, we have

$$p_L(\xi,\eta) - p_{Ph,L} = \int_{\xi,\eta=\delta}^{\xi,\eta} \frac{\partial p_L}{\partial \eta}\partial\eta = \int_{\xi,\eta=\delta}^{\xi,\eta} \frac{\partial p_{disp}}{\partial \eta}\partial\eta.$$

With Eq. (11) we find

$$p_L(\xi,\eta) = p_{Ph,L} + \frac{A_{disp,SL}}{\eta^3} - \frac{A_{disp,SL}}{\delta^3}. \qquad (33)$$

The difference of the two dispersion pressures describes the pressure increase inside the liquid because of the action of dispersion forces on the liquid column of height δ - η. $A_{disp,SL}$ is the dispersion constant for the solid–liquid interaction upon this liquid column. As follows from the combining rules we have

$$A_{\mathrm{disp,SL}} 6\pi = A_{\mathrm{SL}} = \sqrt{A_{\mathrm{SS}} A_{\mathrm{LL}}},$$

which is positive for the wetting liquids considered here. Combining Eq. (33) with Eqs. (20) and (29) yields the pressure distribution in the liquid film

$$p_{\mathrm{L}}(\xi,\eta) = p_{\mathrm{sat}}(T_{\mathrm{Ph}}) - \frac{\rho_{\mathrm{L}}}{\rho_{\mathrm{L}} - \rho_{\mathrm{G}}}\sigma K + \frac{A_{\mathrm{disp,Ph,L}}}{\delta^3} + \frac{A_{\mathrm{disp,SL}}}{\eta^3} - \frac{A_{\mathrm{disp,SL}}}{\delta^3}, \qquad (34)$$

whereas the dispersion constant $A_{disp,SL}$ is positive, $A_{disp,Ph,L}$ is negative as follows from Eq. (21).

5. Experiments

5.1 Experiment 1

N = Number of measurement

V = Volume of water droplet (µl)

φ = Humidity of air (%)

T = Temperature of air (°C)

γ = Remark of the slope angle of plate (°)

N	V	φ	T	Remarks (γ)
	µl	%	°C	°
1	5	37	20,77	59,75
2	5	37,2	20,77	73,92
3	5	36,5	20,45	52,25
4	5	36,5	20,48	45,50
5	5	36,4	20,5	27,50
1	10	36,4	20,6	32
2	10	36,3	20,63	28,08
3	10	36,1	20,58	28,25
4	10	36,4	20,55	24,83
5	10	36,3	20,6	24,33
1	15	36,3	20,65	22
2	15	36,3	20,7	21,75
3	15	41	20,79	32,33
4	15	40,7	20,93	28,66
5	15	41	20,97	41
1	20	40,6	21	25,33
2	20	41,5	21	33,33
3	20	40,5	21,02	35,92
4	20	40,5	21,03	39,25
5	20	40,6	21,03	35,25

N	V	φ	T	Remarks (γ)
	µl	%	°C	°
1	25	40,5	21,11	26,66
2	25	41,6	21,16	23,33
3	25	40,5	21,16	21,16
4	25	40,6	21,16	19
5	25	40,8	21,13	22,58
1	30	40,8	21,1	16,25
2	30	41,1	21,08	17,5
3	30	40,8	21,09	20,42
4	30	40,7	21,1	19,42
5	30	40,8	21,09	21,67
1	35	40,9	21,09	15,25
2	35	41,2	21,06	15,66
3	35	40,9	21,08	16,08
4	35	40,8	21,07	15,5
5	35	40,9	21,07	16,5
1	40	51,2	22,09	14,08
2	40	49,7	22,17	17,33
3	40	49,6	22,21	12,33
4	40	49,6	22,26	11,75
5	40	49,4	22,37	16,83
1	45	49,5	22,35	18,08
2	45	49,4	22,39	15,33
3	45	49,5	22,39	20,92
4	45	49,4	22,39	22,33
5	45	49,5	22,4	18,25
1	50	49,4	22,4	17,25
2	50	49,3	22,4	23,08
3	50	49,3	22,39	15,92
4	50	49,4	22,39	19,83
5	50	49,1	22,41	17,08

5.2 Experiment 2

	N	V	φ	T	Remarks (γ)
		µl	%	°C	°
τ = 2 min					
	1	5	38,7	21,8	56,08
	2	10	38,6	22,02	29,17
	3	15	38,5	22,13	33,08
	4	20	38,4	22,23	31,33
	5	25	38,5	22,35	35,17
	6	30	38,4	22,44	21,67
	7	35	38,2	22,5	19,75
	8	40	38,2	22,55	15,33
	9	45	38,2	22,57	10,5
	10	50	38,4	22,63	11,33
τ = 5 min					
	1	5	35,4	22,33	64,25
	2	10	35,8	22,38	48,17
	3	15	35	22,45	58,08
	4	20	35,5	22,55	32,33
	5	25	35,1	22,57	30,17
	6	30	35,2	22,65	20
	7	35	34,9	22,67	29,5
	8	40	34,9	22,71	17,58
	9	45	34,9	22,76	15,17
	10	50	34,7	22,81	12,25
τ = 10 min					
	1	5	34,8	22,73	61,33
	2	10	34,6	22,93	52,08
	3	15	34,6	23,01	21,33
	4	20	31,7	22,13	18,17
	5	25	32	22,15	28,58
	6	30	31,9	22,19	46,17
	7	35	31,9	22,13	28,25
	8	40	32,1	22,14	25,25
	9	45	32,2	22,1	32,92
	10	50	32,3	22,08	25,33

	N	V	φ	T	Remarks (γ)
		µl	%	°C	°
τ = 15 min					
	1	5	37,2	20,74	44,67
	2	10	37,3	20,83	51,08
	3	15	37,3	20,84	40,17
	4	20	37,3	20,87	32,25
	5	25	32,3	20,69	32,92
	6	30	32,5	20,9	36
	7	35	32,5	21,13	27,25
	8	40	37,4	22,23	21,58
	9	45	37,7	22,41	15,25
	10	50	37,6	22,54	20
τ = 20 min					
	1	5	37,4	22,73	57,25
	2	10	37,2	23,02	62,08
	3	15	39,5	22,87	30,08
	4	20	40	23,06	33,08
	5	25	40,1	23,16	26,25
	6	30	40,2	23,49	32,17
	7	35	40,3	23,34	31,25
	8	40	40,3	23,43	24,08
	9	45	40,1	23,56	30
	10	50	40,1	23,61	23

6. Experimental data

6.1 Experiment 1

6.1.1 Evaluation of the data

All data of this experiment have been evaluated in each case (µm = 5, 10, 15, 20, 25, 30, 35, 40, 45, 50) in order that the last graphs give us the most precise and specific information possible. The process has been the next for each volume of water droplet:

$$\gamma_1, \gamma_2, \gamma_3, \gamma_4, \gamma_5$$

$$\gamma_{AVERAGE} = \frac{\sum_{i=1}^{5} \gamma i}{5}$$

$$\Delta\gamma_i = \gamma_{AVERAGE} - \gamma_i$$

Once $\Delta\gamma_i$, the range (σ) is calculated:

$$\sigma = \sqrt{\frac{\sum_{i=1}^{n} \Delta\gamma i}{(n-1)}}$$

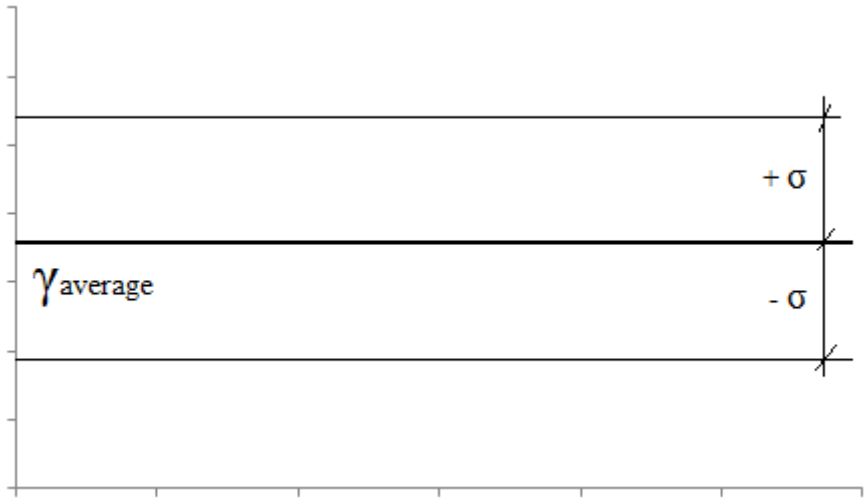

When σ is calculated, we can know the dispersion of the values from the $\gamma_{average}$. If there is any value that it is far away from the range (σ), this value must be deleted and with the rest correct values of the experiment, we have to calculate again the average parameters (φ, T, γ) which we will put in graphs.

Nomenclature

N = Number of measurement

V = Volume of water droplet (µl)

φ = Humidity of air (%)

T = Temperature of air (°C)

γ = Remark of the slope angle of plate (°)

µl = 5

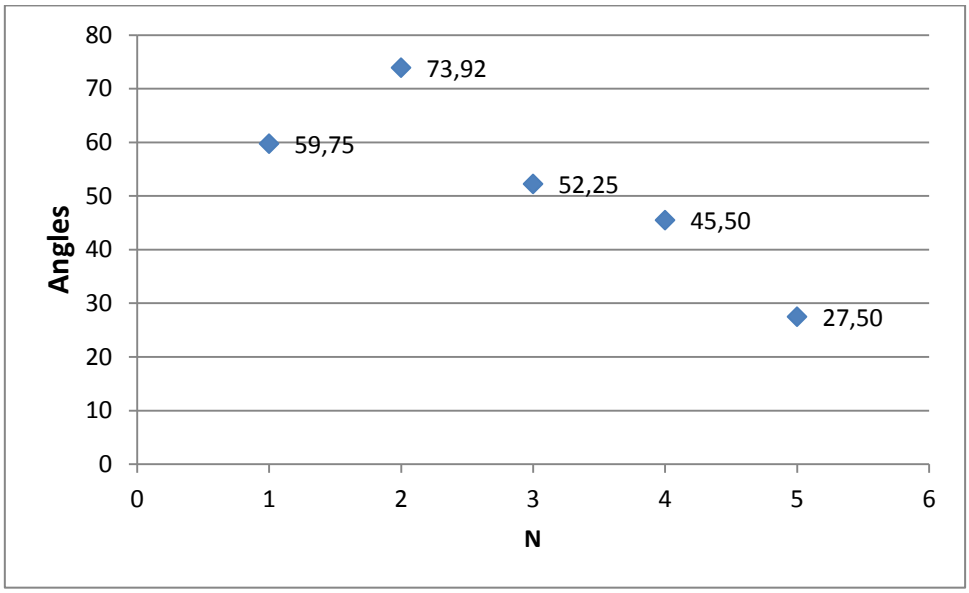

$\gamma_{average}$	51,78
σ	3,91
γ + σ	55,69
γ - σ	47,87

N	V	φ	T	Remarks (γ)
	µl	%	°C	°
1	5	37	20,77	59,75
2	5	37,2	20,77	73,92
3	5	36,5	20,45	52,25
4	5	36,5	20,48	45,50
5	5	36,4	20,5	27,50

Average	36,67	20,57	52,50

µl = 10

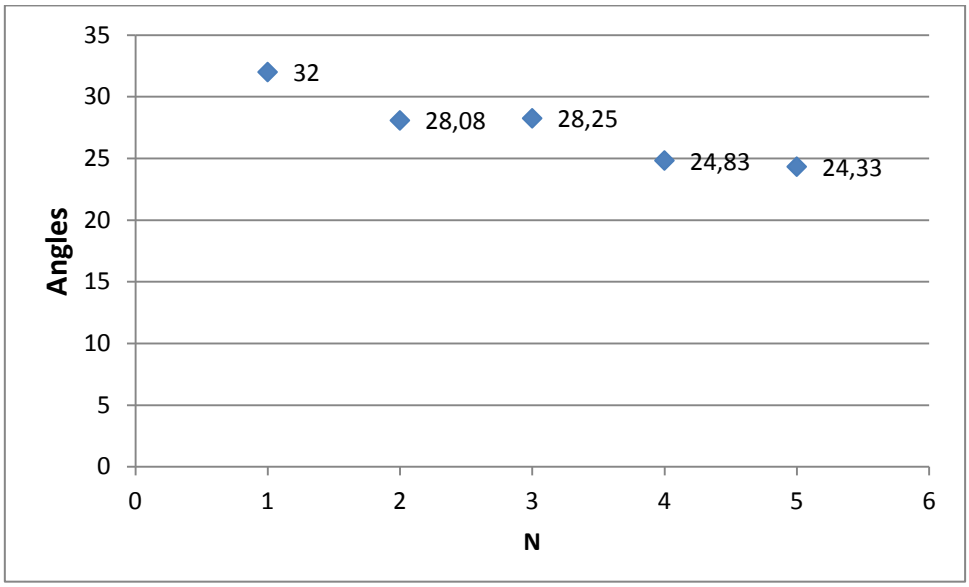

$\gamma_{average}$	27,50
σ	1,71
γ + σ	29,21
γ - σ	25,79

N	V	φ	T	Remarks (γ)
	µl	%	°C	°
1	10	36,4	20,6	32
2	10	36,3	20,63	28,08
3	10	36,1	20,58	28,25
4	10	36,4	20,55	24,83
5	10	36,3	20,6	24,33

Average	36,28	20,59	26,37

µl = 15

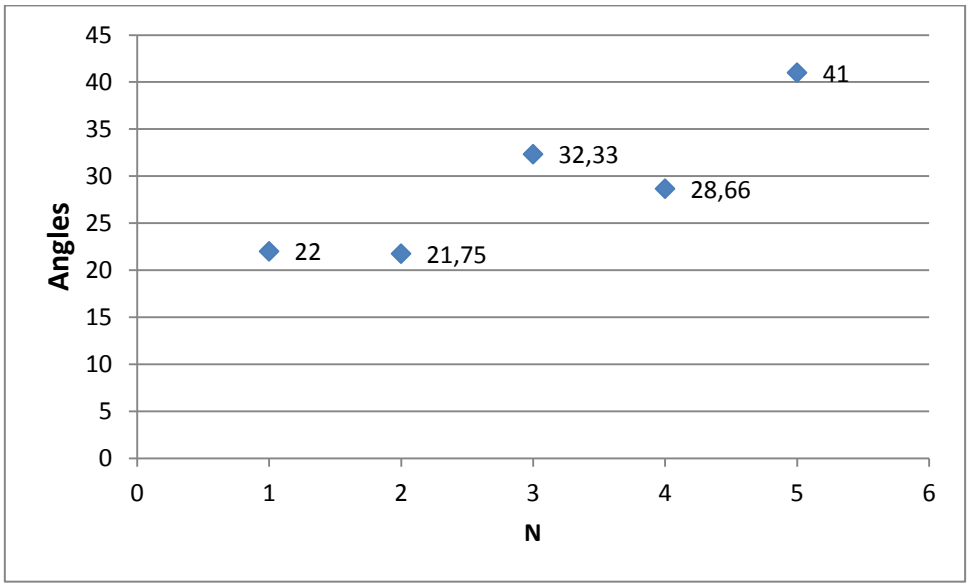

$\gamma_{average}$	29,15
σ	2,74
γ + σ	31,89
γ - σ	26,41

N	V	φ	T	Remarks (γ)
	µl	%	°C	°
1	15	36,3	20,65	22
2	15	36,3	20,7	21,75
3	15	41	20,79	32,33
4	15	40,7	20,93	28,66
5	15	41	20,97	41

Average	38,58	20,77	26,19

µl = 20

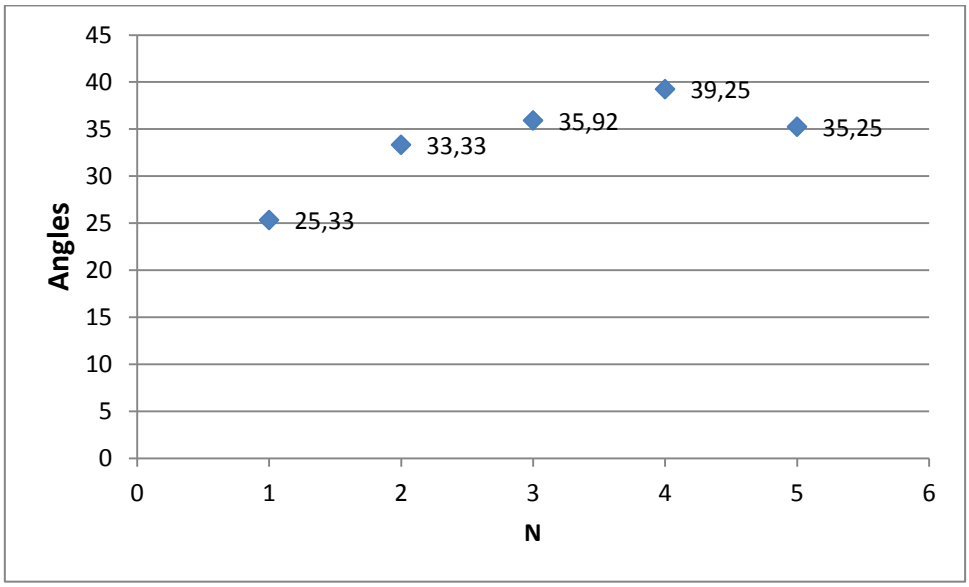

$\gamma_{average}$	33,82
σ	2,12
γ + σ	35,93
γ - σ	31,70

N	V	φ	T	Remarks (γ)
	µl	%	°C	°
1	20	40,6	21	25,33
2	20	41,5	21	33,33
3	20	40,5	21,02	35,92
4	20	40,5	21,03	39,25
5	20	40,6	21,03	35,25

Average	40,775	21,02	35,9375

µl = 25

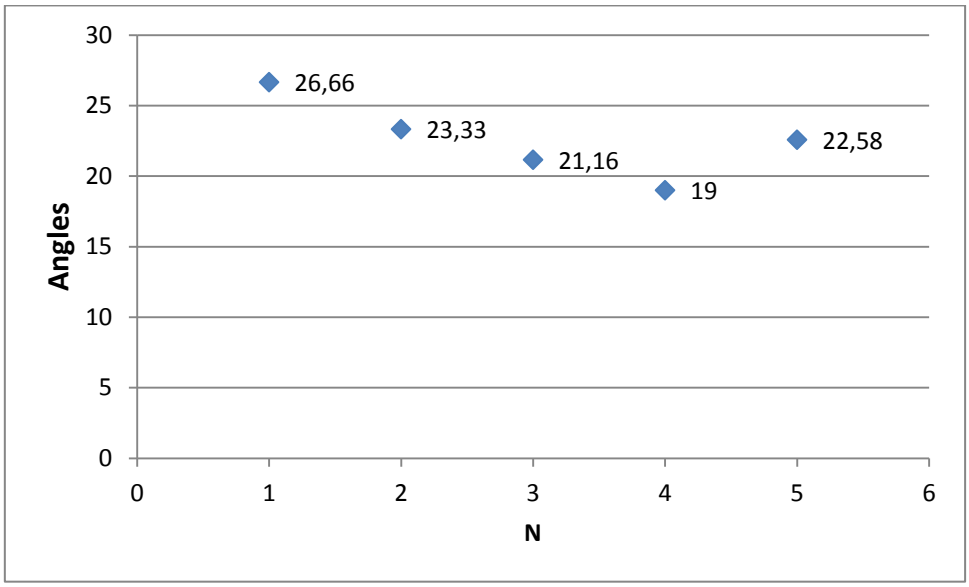

$\gamma_{average}$	22,55
σ	1,57
γ + σ	24,12
γ - σ	20,98

N	V	φ	T	Remarks (γ)
	µl	%	°C	°
1	25	40,5	21,11	26,66
2	25	41,6	21,16	23,33
3	25	40,5	21,16	21,16
4	25	40,6	21,16	19
5	25	40,8	21,13	22,58

Average	40,8	21,14	22,55

µl = 30

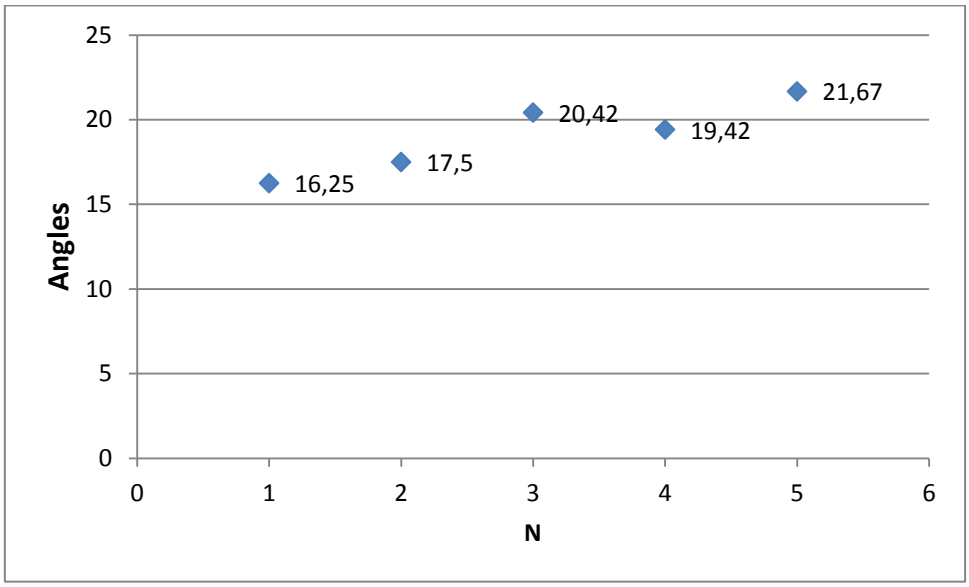

$\gamma_{average}$	19,05
σ	1,48
γ + σ	20,53
γ - σ	17,58

N	V	φ	T	Remarks (γ)
	µl	%	°C	°
1	30	40,8	21,1	16,25
2	30	41,1	21,08	17,5
3	30	40,8	21,09	20,42
4	30	40,7	21,1	19,42
5	30	40,8	21,09	21,67

Average	40,84	21,09	19,05

µl = 35

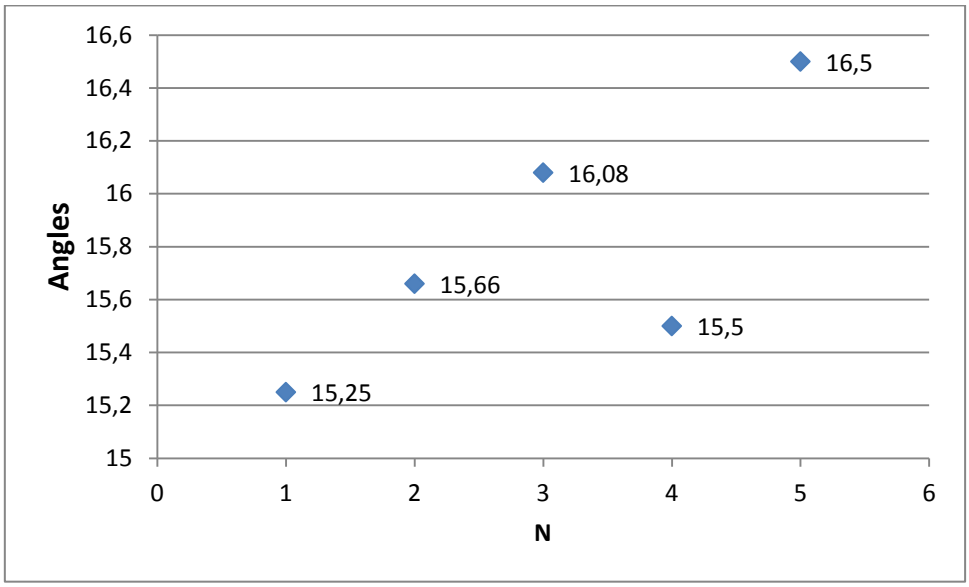

$\gamma_{average}$	15,80
σ	0,70
γ + σ	16,50
γ - σ	15,10

N	V	φ	T	Remarks (γ)
	µl	%	°C	°
1	35	40,9	21,09	15,25
2	35	41,2	21,06	15,66
3	35	40,9	21,08	16,08
4	35	40,8	21,07	15,5
5	35	40,9	21,07	16,5

Average	40,94	21,07	15,80

µl = 40

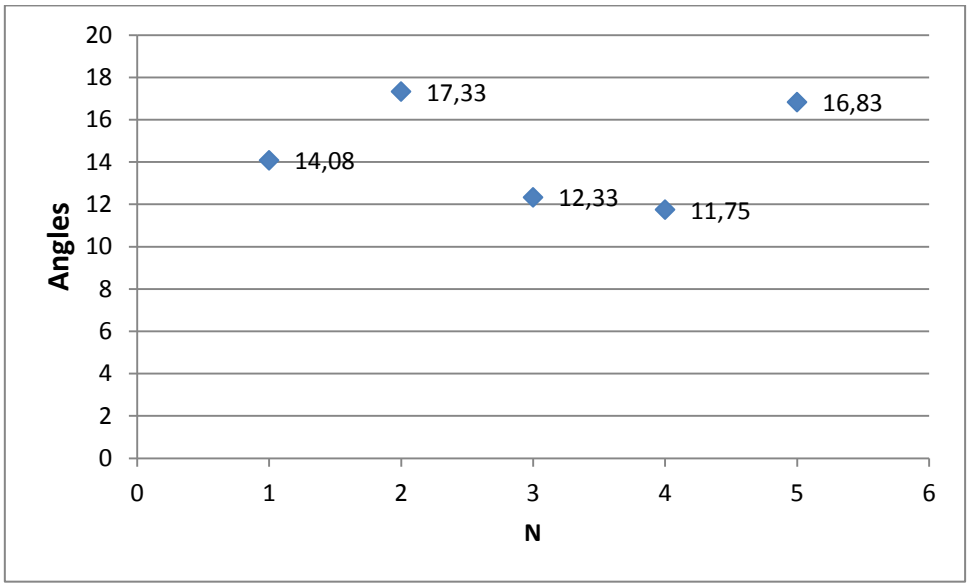

$\gamma_{average}$	14,46
σ	1,62
γ + σ	16,08
γ - σ	12,85

N	V	φ	T	Remarks (γ)
	µl	%	°C	°
1	40	51,2	22,09	14,08
2	40	49,7	22,17	17,33
3	40	49,6	22,21	12,33
4	40	49,6	22,26	11,75
5	40	49,4	22,37	16,83

Average	49,9	22,22	14,46

µl = 45

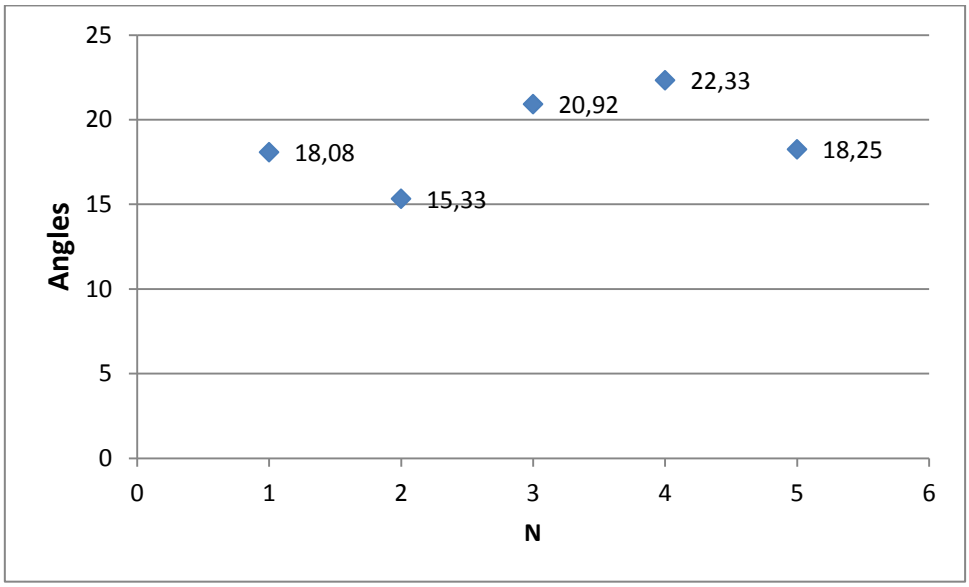

$\gamma_{average}$	18,98
σ	1,63
γ + σ	20,61
γ - σ	17,36

N	V	φ	T	Remarks (γ)
	µl	%	°C	°
1	45	49,5	22,35	18,08
2	45	49,4	22,39	15,33
3	45	49,5	22,39	20,92
4	45	49,4	22,39	22,33
5	45	49,5	22,4	18,25

Average	49,46	22,38	18,98

µl = 50

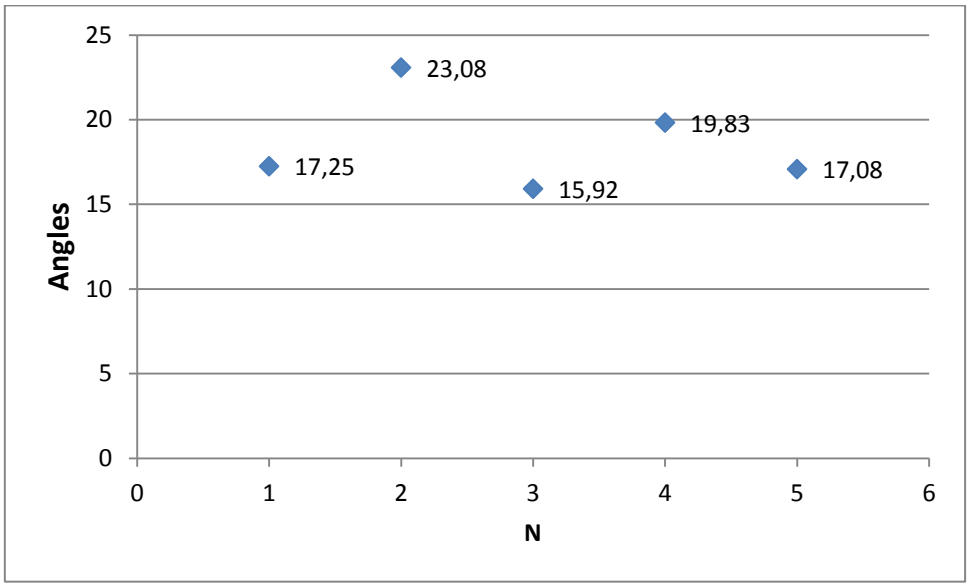

$\gamma_{average}$	18,63
σ	1,68
γ + σ	20,31
γ - σ	16,95

N	V	φ	T	Remarks (γ)
	µl	%	°C	°
1	50	49,4	22,4	17,25
2	50	49,3	22,4	23,08
3	50	49,3	22,39	15,92
4	50	49,4	22,39	19,83
5	50	49,1	22,41	17,08

Average	49,3	22,40	17,52

First graph: $\gamma_{average}$ - $\varphi_{average}$

γ AVERAGE (°)	φ AVERAGE (%)
52,5	36,67
26,37	36,28
26,19	38,58
35,94	40,775
22,55	40,8
19,05	40,84
15,8	40,94
14,46	49,9
18,98	49,46
17,52	49,3

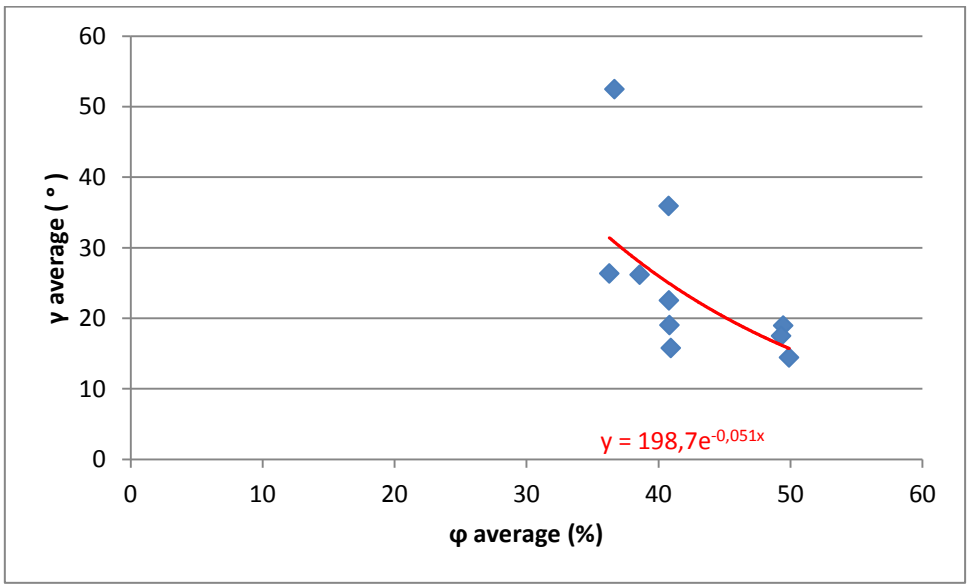

- The graphic shows that the slope angle oh plate depends on the humidity of the air. When the humidity increases, the slope angle of plate decreases.

Second graph: $\gamma_{average}$ - $T_{average}$

γ AVERAGE (°)	T AVERAGE (°C)
52,5	20,57
26,37	20,59
26,19	20,77
35,94	21,02
22,55	21,14
19,05	21,09
15,8	21,07
14,46	22,22
18,98	22,38
17,52	22,4

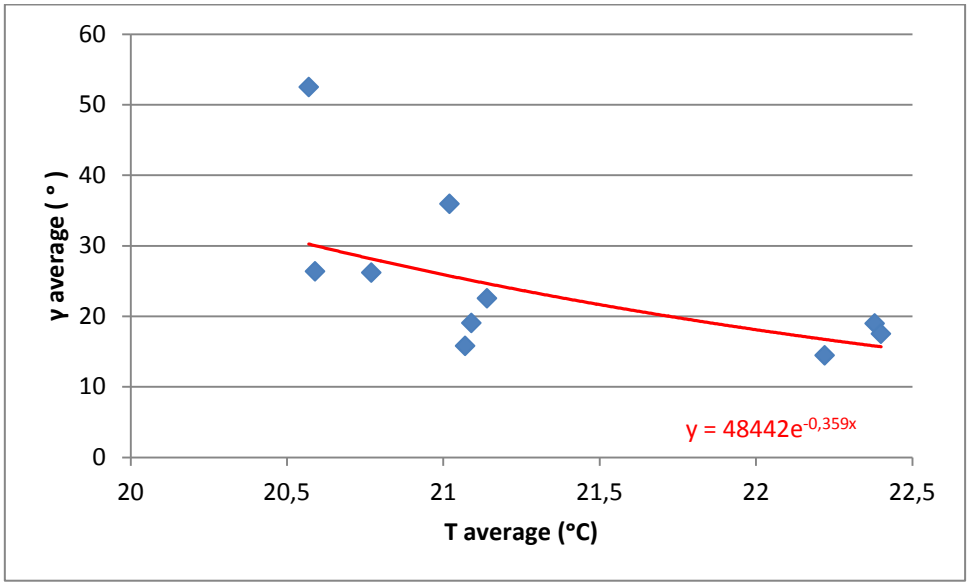

- This graphic shows that the slope angle of plate depends on the temperature of air. When temperature increases, the slope angle of plate decreases.
  But the range of temperature is very small (about 2 °C) and this conclusion can be wrong, it is only a supposition.

Third graph: $\gamma_{average}$ - V

γ AVERAGE (°)	V (µl)
52,5	5
26,37	10
26,19	15
35,94	20
22,55	25
19,05	30
15,8	35
14,46	40
18,98	45
17,52	50

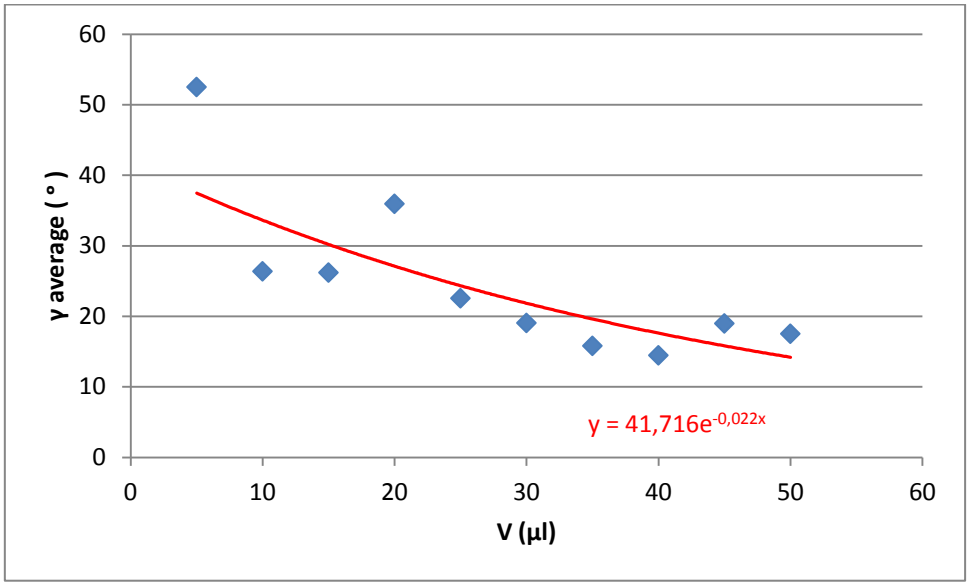

- This graphic shows that the slope angle of plate depends on the volume of water droplet.

  When volume increases, the slope angle of plate decreases.

6.2 Experiment 2

τ = 2 min

V (µl)	γ (°)
5	56,08
10	29,17
15	33,08
20	31,33
25	35,17
30	21,67
35	19,75
40	15,33
45	10,5
50	11,33

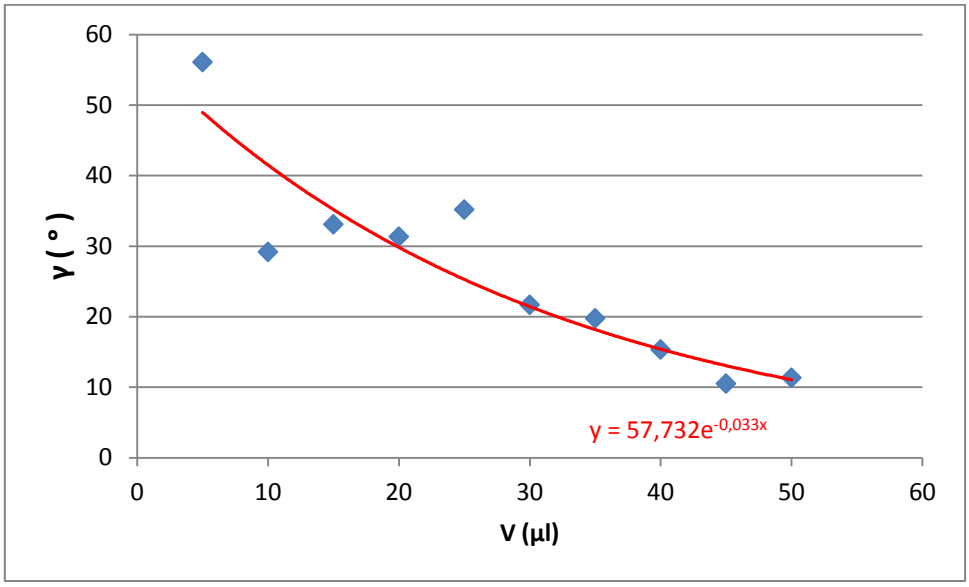

τ = 5 min

V (µl)	γ (°)
5	64,25
10	48,17
15	58,08
20	32,33
25	30,17
30	20
35	29,5
40	17,58
45	15,17
50	12,25

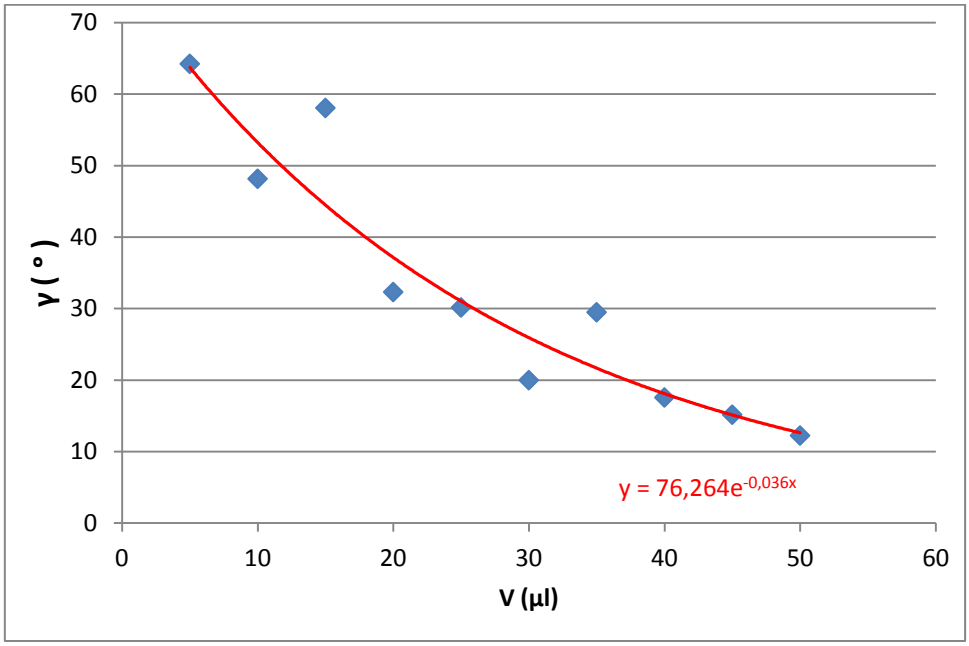

τ = 10 min

V (µl)	γ (°)
5	61,33
10	52,08
15	21,33
20	18,17
25	28,58
30	46,17
35	28,25
40	25,25
45	32,92
50	25,33

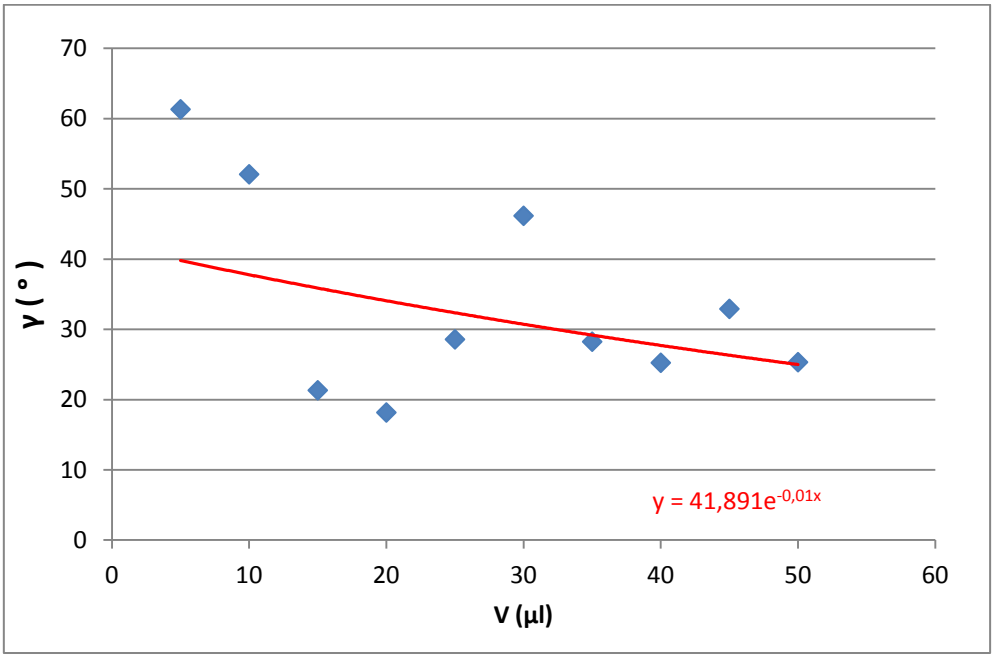

τ = 15 min

V (µl)	γ (°)
5	44,67
10	51,08
15	40,17
20	32,25
25	32,92
30	36
35	27,25
40	21,58
45	15,25
50	20

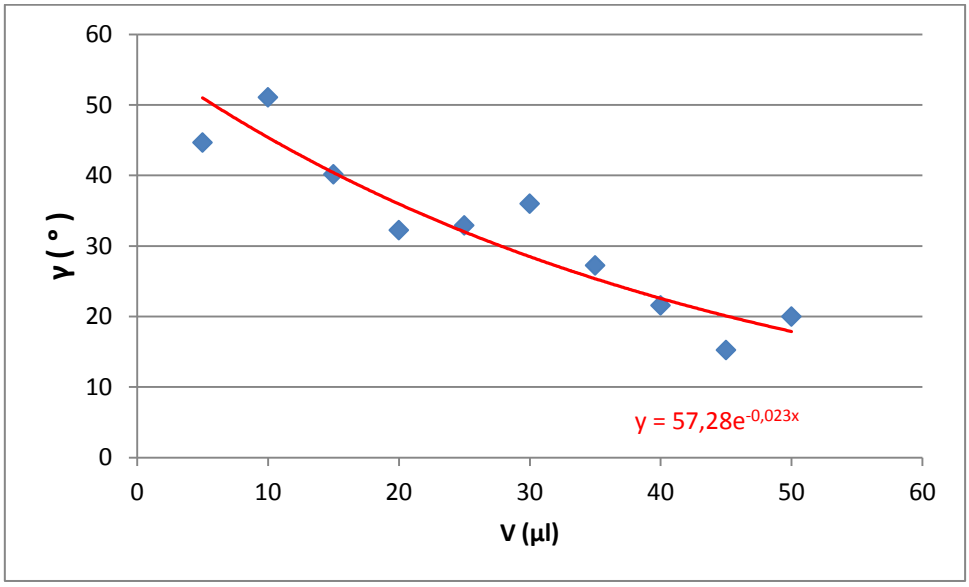

τ = 20 min

V (µl)	γ (°)
5	57,25
10	62,08
15	30,08
20	33,08
25	26,25
30	32,17
35	31,25
40	24,08
45	30
50	23

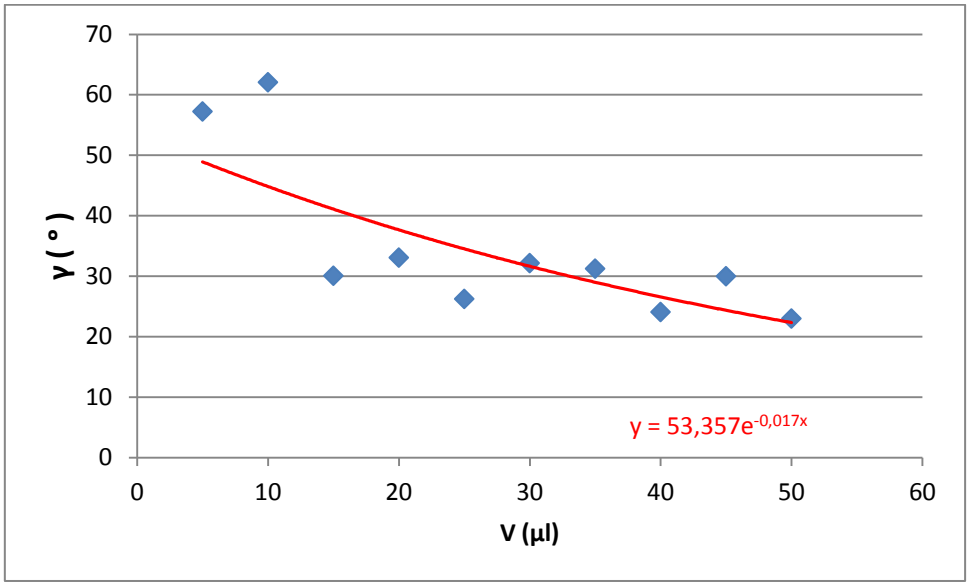

7. Evaluated of microfilm thickness (Vladimir S. Ajaev)

7.1 Introduction

The evolution of a liquid droplet that spreads on a solid surface is known to depend on the local conditions near the contact line where the surface of the droplet touches the solid. Incorporating such local conditions into the standard description of viscous flow in the liquid results in a non-physical shear-stress singularity which can be removed by relaxing the no-slip condition for the viscous flow or introducing a microscopic precursor film.

Adding the effect of evaporation at the droplet surface may be expected to further complicate the problem and thus require some additional modeling assumptions. As we show below, this is not necessarily the case since evaporation alters the flow structure and thus allows us to employ mathematical models which are not appropriate for the isothermal case.

The goal of this paper is to investigate moving contact lines in the presence of evaporation in the context of spreading and develop a mathematical model that does not involve any *ad hoc* assumptions about the value of the apparent contact angle. Developing such a model is especially important since moving contact lines in applications often appear when evaporation is also significant.

Spreading can be analysed using a lubrication-type approach if droplet thickness is much smaller than its radius, as shown by Lopez, Miller & Ruckenstein (1976) and Greenspan (1978) for isothermal spreading. They took into account viscous and capillary effects and reduced the problem to a single partial differential equation for droplet thickness.

A detailed investigation of the effect of different contact line models on droplet spreading was carried out by Haley & Miksis (1991). Additional physical effects, such as Marangoni stresses at the droplet surface and chemical reaction at the solid–liquid interface, were investigated later for non-volatile droplets in the framework of the same approach by Ehrhard & Davis (1991) and Braun et al. (1995). Experimental results for spreading of silicon oil on glass (Ehrhard 1993) are in agreement with the lubrication-type models.

The effect of evaporation in droplet spreading was considered by Anderson & Davis (1995) in the framework of the lubrication theory for a two-dimensional model. They used the one-sided model of evaporation which implies that all dynamical processes in the vapour are negligible. Corrections to the equilibrium value of the contact angle owing to contact-line motion and evaporation are both assumed relatively small and therefore their linear superposition is used to determine the contact angle.

The dynamic contribution to the contact angle (owing to the flow near the moving contact line) is approximated by a linear relation between the speed and the cube of the contact-angle departure from the equilibrium value. Later, Hocking (1995) suggested that a different model for the dynamic contribution to the contact angle is more appropriate, but used the same superposition principle to investigate the combined effect of evaporation and fluid flow on the contact-line motion.

Formulae for the corrections to the equilibrium value of the contact angle due to contact line motion in both papers are motivated by experiments with no evaporation at the droplet surface.

In the present work, we use a different approach to contact-line modelling suggested by Potash & Wayner (1972) and Moosman & Homsy (1980) in their studies of steady contact lines on heated surfaces. It relies on the description of dry areas on heated surfaces by microscopic adsorbed films which are in thermodynamic equilibrium with both solid and vapour phases.

Such equilibrium can be achieved for non-zero film thickness owing to action of London–van der Waals forces. The pressure in the film due to these forces is inversely proportional to the cube of film thickness. We note that the adsorbed film is introduced here, not as an artificial tool needed to remove the singularity at the contact line, but rather as a physical effect with experimental verification.

The adsorbed film is always formed on the solid surface if the droplet is surrounded by vapour. A macroscopic interfacial shape, such as liquid film or constant-curvature meniscus, has to approach the adsorbed-film solution when the macroscopically dry region is approached. The contact line is then defined as the region of rapid change of interfacial curvature where the transition between the macroscopic shape and the adsorbed film takes place.

The approach has been used successfully by DasGupta et al. (1993) and Morris (2001) for finding local solutions near the contact lines on heated surfaces and by Ajaev & Homsy (2001) for finding global shapes of steady vapour bubbles in microchannels. It has not been applied to spreading of volatile liquids on heated surfaces even though microscopic films are often used in models of isothermal spreading (de Gennes 1985; Glasner 2003).

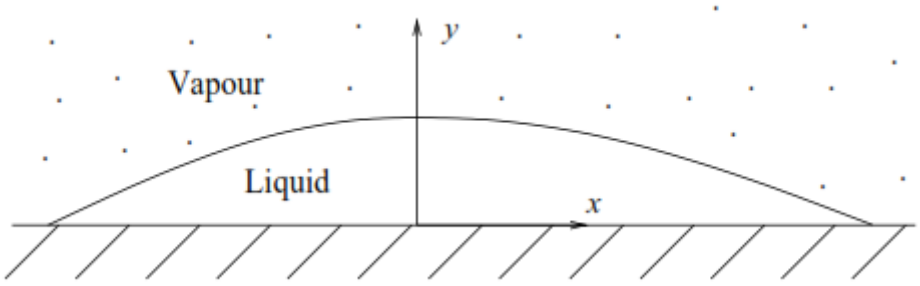

Fig. 1. A sketch of a thin volatile droplet spreading on a uniformly heated surface. Cartesian coordinates are shown.

This approach was originally developed for liquids which are perfectly wetting under isothermal conditions. One of the main challenges in modelling contact lines with evaporation is to generalize this approach to the case of partial wetting. The assumption that the disjoining pressure is an inverse power of the film thickness is no longer applicable for this case.

Two different approaches can be taken. We can use an experimentally motivated disjoining pressure curve that accounts for both attractive and repulsive interactions; the contact angle is then related to the area under this curve.

Alternatively, we can derive a slope-dependent expression for the disjoining pressure near the contact line by integrating over all intermolecular interactions with a simple model potential and a cut off length, following Miller & Ruckenstein (1974), Hocking (1993) and Wu & Wong (2004). The latter approach is taken in the present work. We believe that both approaches are capable of describing experimental results, but we do not attempt a detailed comparison here.

In the present work, we develop a model of spreading of a droplet of either perfectly or partially wetting volatile liquid on a uniformly heated surface. The droplet is in direct contact with a large reservoir of vapour. The model incorporates the effects of surface tension, gravity, evaporation, thermocapillarity and disjoining pressure in the framework of a lubrication-type approach.

We note that many previous theoretical investigations of spreading have been carried out in the framework of two-dimensional models, while axisymmetric shapes are clearly more relevant experimentally. Therefore, we first present a complete formulation of the problem and discuss the several important results in the framework of a two-dimensional model to facilitate an easy comparison with the previous work.

7.2 Formulation

We consider a two-dimensional droplet of a volatile liquid of density ρ and viscosity μ on a uniformly heated rigid surface, as shown in figure 1. The fluid flow in the vapour phase directly above the liquid is, in general, coupled to the liquid flow in the droplet. However, in this study, we use the one-sided model of evaporation of Burelbach, Bankoff & Davis (1988).

It implies that the density, dynamic viscosity and thermal conductivity of the vapour phase are very small compared to those of the liquid. Therefore, we take the limit when the corresponding non-dimensional ratios approach zero. However, the vapour density is retained in the boundary conditions where it multiplies the vapour velocity, which can be large.

We define the capillary number according to

$$C = \frac{\mu U}{\sigma_0}, \qquad (1)$$

where σ_o is the surface tension at the equilibrium saturation temperature, T_S^*, and the characteristic velocity is determined from the interfacial mass balance as

$$U = \frac{kT_s^*}{\rho \mathscr{L} R_0}. \qquad (2)$$

Here, k is the thermal conductivity of the liquid, L is the latent heat of vaporization per unit mass, and R_0 is the initial radius of the droplet.

Let us consider the limit of small capillary numbers. In order to obtain physically meaningful solutions, we consider distinguished limits when physical quantities, as well as parameters of the problem, scale as certain powers of the capillary number. Solutions are obtained from the leading-order terms of an asymptotic expansion in powers of $C^{1/3}$.

We note that it is often convenient to consider an asymptotic expansion in terms of an aspect ratio of the droplet. However, the cube of the aspect ratio has to scale as the capillary number in order for this approach to result in experimentally relevant solutions, so it is essentially equivalent to our asymptotic expansion in powers of $C^{1/3}$.

For simplicity we carry out the derivation for a perfectly wetting liquid with disjoining pressure being inversely proportional to the cube of the thickness of the liquid layer on the solid surface. A more general case of the slope-dependent disjoining pressure is discussed briefly in the end of the next section.

Let us choose the length scales in the horizontal and vertical directions as R_0 and $C^{1/3}R_0$, respectively; the resulting non-dimensional Cartesian coordinate system, (x, y), is shown in figure 1. The vapour–liquid interface in our formulation is represented by a function y =h(x, t), where t is the time variable scaled by R_0/U. We choose $C^{1/3}U$ as the velocity scale in the y-direction and $C^{1/3}\sigma_0 / R_0$ as the pressure scale. The governing equations at leading order take the usual lubrication-type form:

$$-p_x + u_{yy} = 0, \tag{3}$$
$$-p_y - B = 0, \tag{4}$$
$$u_x + v_y = 0, \tag{5}$$
$$T_{yy} = 0. \tag{6}$$

Here, $B = \rho g R_0^2/\sigma_0$ is the Bond number, g is the acceleration due to gravity; the velocity in the x-direction is scaled by U, the non-dimensional temperature T is defined in terms of the dimensional one, T^*, according to

$$T = \frac{T^* - T_S^*}{C^{2/3}T_S^*}. \tag{7}$$

Let us now turn to the interfacial boundary conditions. In order to include the non-dimensional evaporative mass flux J into the leading-order mass-conservation condition, we scale the dimensional flux by $\rho U C^{1/3}$. With this choice and the above length and velocity scales, the non-dimensional leading-order conditions for conservation of mass and energy at the interface are written in the form:

$$J + uh_x - v = -h_t, \tag{8}$$
$$J = -T_y. \tag{9}$$

Equation (9) can be interpreted as the balance between the heat conducted through the droplet and the latent heat of the phase change at the interface. Heat transfer from the liquid film to the vapour is assumed negligible here, but it can be easily accounted for in the framework of our approach. The normal stress condition at the interface includes contributions from capillarity and disjoining pressure:

$$p - p_v = -h_{xx} - \frac{\varepsilon}{h^3}, \qquad (10)$$

where p_v is the non-dimensional vapour pressure. We assume that the disjoining pressure is inversely proportional to the cube of film thickness and introduce a nondimensional parameter, $\varepsilon = |A| / (\sigma_0 R_0^2 C)$ which is assumed to be an order of one quantity in the asymptotic limit $C \rightarrow 0$, although its numerical value may be small ($\sim 10^{-3}$) ; A is the Hamaker constant.

We assume that the surface tension is a linear function of temperature,

$$\sigma = \sigma_0 - \gamma(T^* - T_S^*), \qquad (11)$$

and introduce the modified Marangoni number $M = \gamma T_S^* / \sigma_0$. We note that this parameter is sometimes referred to as the capillary number, but in our case it is essentially equivalent to the modified Marangoni number introduced by Gramlich et al. (2002) for thin-film flows over topographic features. With this choice, the shear stress condition at the interface is written as

$$u_y = -M(T_x + h_x T_y). \qquad (12)$$

The scaled interfacial temperature T^i is related to the local mass flux and pressure jump at the interface through the non-equilibrium condition, which can be written in the following form:

$$KJ = \delta(p - p_v) + T^i, \qquad (13)$$

where

$$K = \frac{\rho U \sqrt{2\pi \bar{R} T_s^*}}{2\rho_v \mathscr{L} C^{1/3}}, \qquad \delta = \frac{\sigma_0}{\mathscr{L} \rho R_0 C^{1/3}}. \tag{14}$$

Here, R is the gas constant per unit mass, ρ_v is the vapour density. According to (13), the departures of local temperature at the interface from the equilibrium value are characterized by two non-dimensional parameters, K and δ. The kinetic parameter, K, measures the relative importance of kinetic effects at the interface. The parameter δ characterizes the effect of changes in liquid pressure on the local phase-change temperature at the interface.

Derivation of (13) is based on a simple linear relation between the mass flux and the vapour pressure. We note that alternative approaches have been suggested in the literature (Rose 2000), but we do not attempt to review them here.

At the solid–liquid interface, the liquid velocity is zero and the non-dimensional value of the temperature is fixed at $T = T_0 > 0$. The non-dimensional temperature T_0 is an important control parameter in experiments.

7.3 Calculations

Thickness of adsorbed film from equation given by Ajaev:

$$\delta = 9{,}4181 * 10^{-10} * (R_0)^{-1/3}$$

where

$$R_0 = \beta\, r_0$$

$$\beta = B \left(\frac{We}{6} + 2 \right)^{0{,}5}$$

For water droplet B = 0,87.

If the water droplet is slowly deposition on the surface than the Weber number is equal near zero (We ≈ 0).

Spreading factor is equal: β ≈ 1,2304

$$r_0 = \left(\frac{3\,Vo}{4\,\pi} \right)^{1/3}$$

For each volume of droplet, it is calculated the thickness of microfilm correspondent:

V_0 (nl)	r_0	R_0	δ
10^{-9} m^3	10^{-3} m	10^{-3} m	nm
5	1,0608	1,3052	8,6180
10	1,3365	1,6444	7,9792
15	1,5299	1,8824	7,6277
20	1,6839	2,0719	7,3877
25	1,8139	2,2318	7,2068
30	1,9276	2,3717	7,0623
35	2,0292	2,4967	6,9423
40	2,1216	2,6104	6,8401
45	2,2065	2,7149	6,7512
50	2,2854	2,8119	6,6726

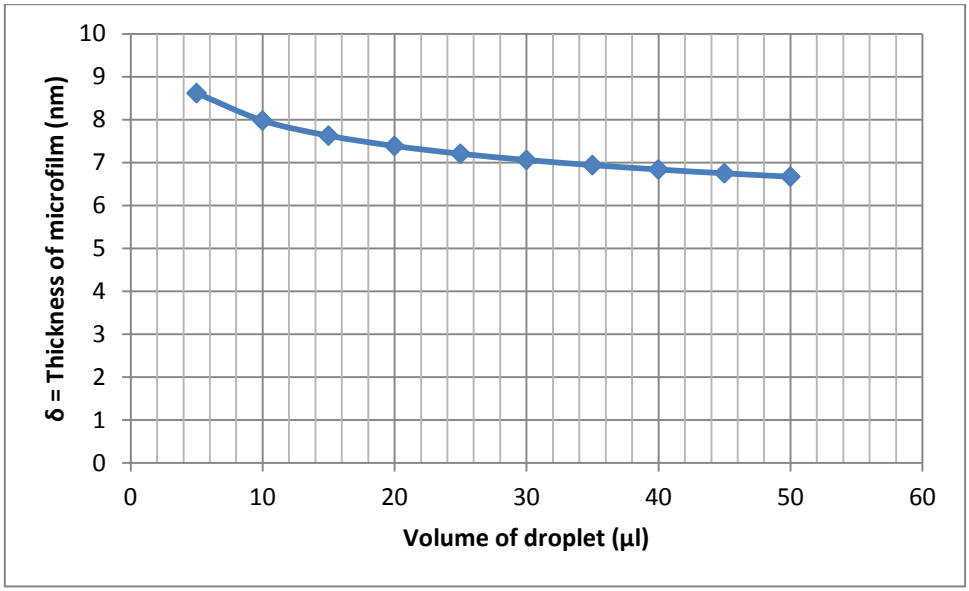

8. Comparison with experimental results

8.1 Model

The model takes into account the effect of intermolecular forces in interfacial regions. Fig. 1. presents a macroscope view of the droplet in the phase of its maximal spreading on the surface liquid microfilm that is coating the solid body surface.

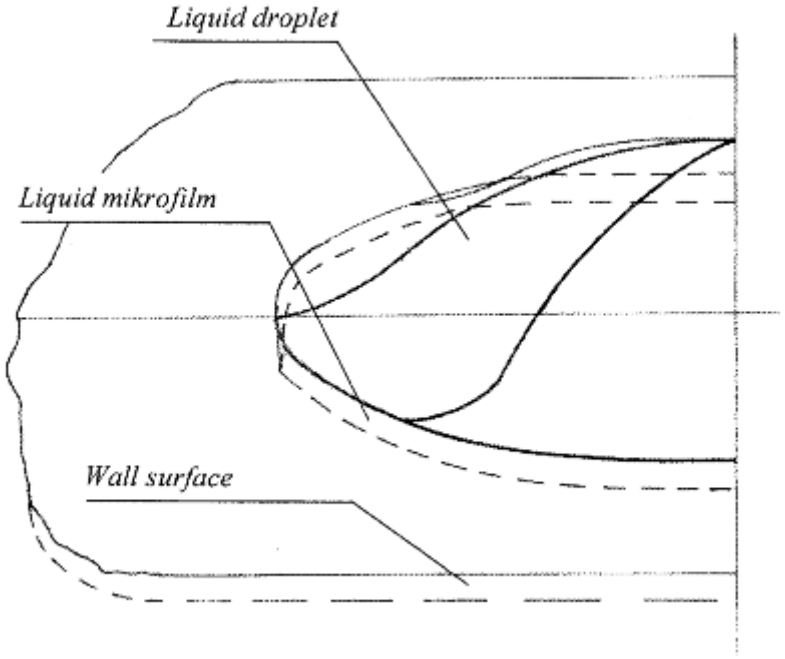

Fig. 1. View of a droplet on the surface of the thin liquid microfilm that is coating the solid body surface

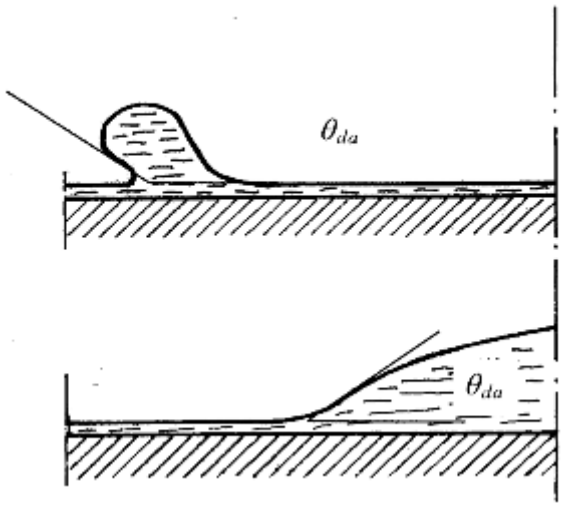

Fig. 2. Shape and dynamic advanced angle in relation to droplet´s spreading dynamics

In the above phase of droplet´s spreading, shape and dynamic advanced angle are essential parameters. They depend on the dynamic of the process (Fig. 2.). If the phenomenon is analysed in macroscopic way, and droplet is characterized with initial energy and thus with high Weber number before its contact with the surface, dynamic advanced angle is an obtuse angle.

With small Weber numbers, dynamic angle can be expected to be an acute angle.. In turn, if the solid body surface is coated with a liquid film, dynamic contact angle close to absorbed liquid microfilm must always be an acute angle, irrespectively of droplet´s spreading dynamic.

Transition of interfacial region of the main part of droplet into a thin liquid film coating the flat surface of a solid boy must occur gently. The acute angle has been called dynamic microscopic advanced angle and denoted as $\theta_{da\,m}$ (Fig.3).

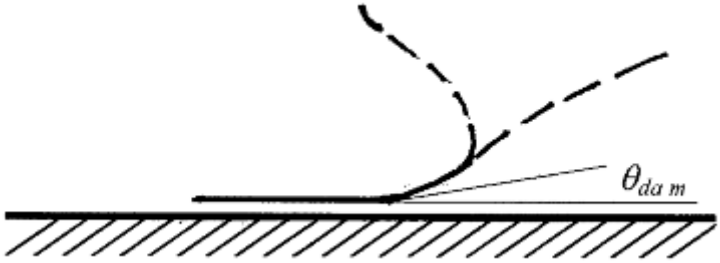

Fig. 3. Dynamic microscopic advanced angle

In the moment when droplet´s spreading stops, quasi-equilibrium state occurs between the region of absorbed liquid film and the micro-region. In order to find out conditions for the above state, the following simplifying assumptions have been accepted:

- The surface is horizontal, smooth, heterogenic and free from micro-impurities
- Surface is coated with a thin liquid film on which the liquid spreads
- There occur no thermal interrelations among the surface, droplet and environment; the process al liquid´s spreading is of isothermal
- Liquid is homogeneous

- As a result of intermolecular forces in the liquid-gas interfacial region, additional pressure called disjoining pressure appears in the liquid micro-film and in the micro-region.
- It is assumed that van der Waals forces have a prevailing effect on the value of intermolecular forces.

Control volume of liquid (Fig. 4) is separated from its micro-region. The volume is limited by two planes perpendicular to the solid body surface and running through droplet´s symmetry axis. They cross each other at angle dφ.

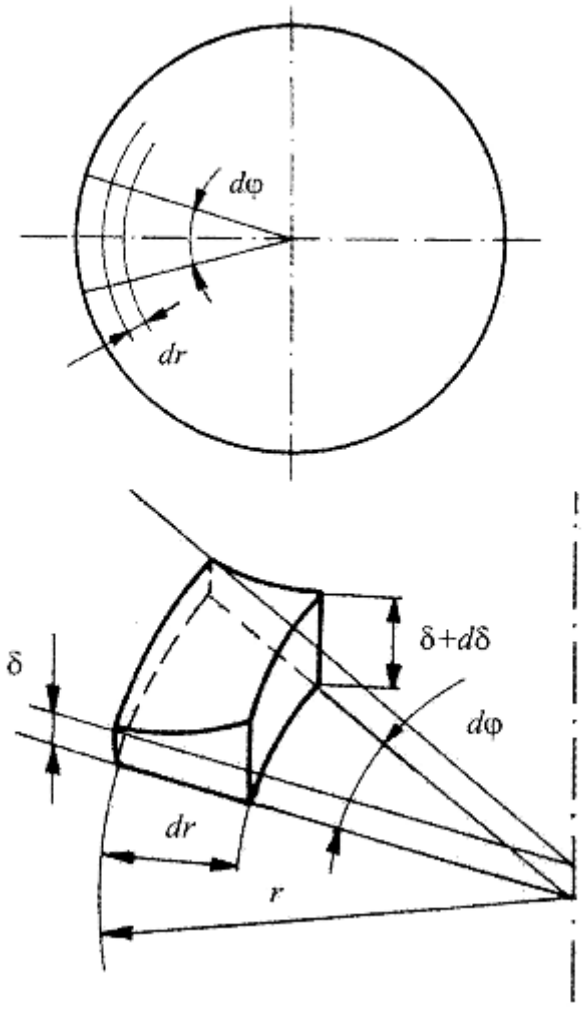

Fig. 4. Control volume of liquid

Next two limiting planes are cylindrical, with radiuses *r* and *(r-dr)*, respectively. Element of liquid´s volume is restricted from the lower side by plane parallel to hypothetic solid body surface and from the upper side by curved interfacial surface liquid-gas. It is assumed in further analysis that upper surface limiting the element of volume is conic, declined at angle α. It is also assumed that liquid´s pressure equals the pressure present on interfacial surface liquid-gas.

The formula of dynamic microscopic advanced angle is the next:

$$\operatorname{tg} \theta_{da\ m} = \frac{\rho\, g\, \delta}{2\, A} \operatorname{tg} \gamma$$

where

ρ = density of water = 998,3 Kg/m^3

g = gravity = 9,81370 m/s^2 (with latitude and height above sea level of Szczecin)

A = A_{dysp} = A_{ham} / 6π

A_{ham} = 5,86*10^{-20} J

The results of slope angle of plate using volume of droplet equal **20 µl** in this model, are given in the next table:

Items	γ (°)	Items	γ (°)
1	31,75	13	50,17
2	43	14	33
3	37,25	15	29,83
4	52	16	20
5	53	17	21,5
6	21	18	23,92
7	20	19	24
8	21,5	20	39,17
9	35,33	21	24,66
10	34,5	22	40,83
11	27,67	23	36
12	34	24	46,25

$$\gamma_{average} = 33{,}35\ °$$

The next graph show the relation between tangent of dynamic microscopic advanced angle in relation to slope angle of the plate and to thickness of the liquid film.

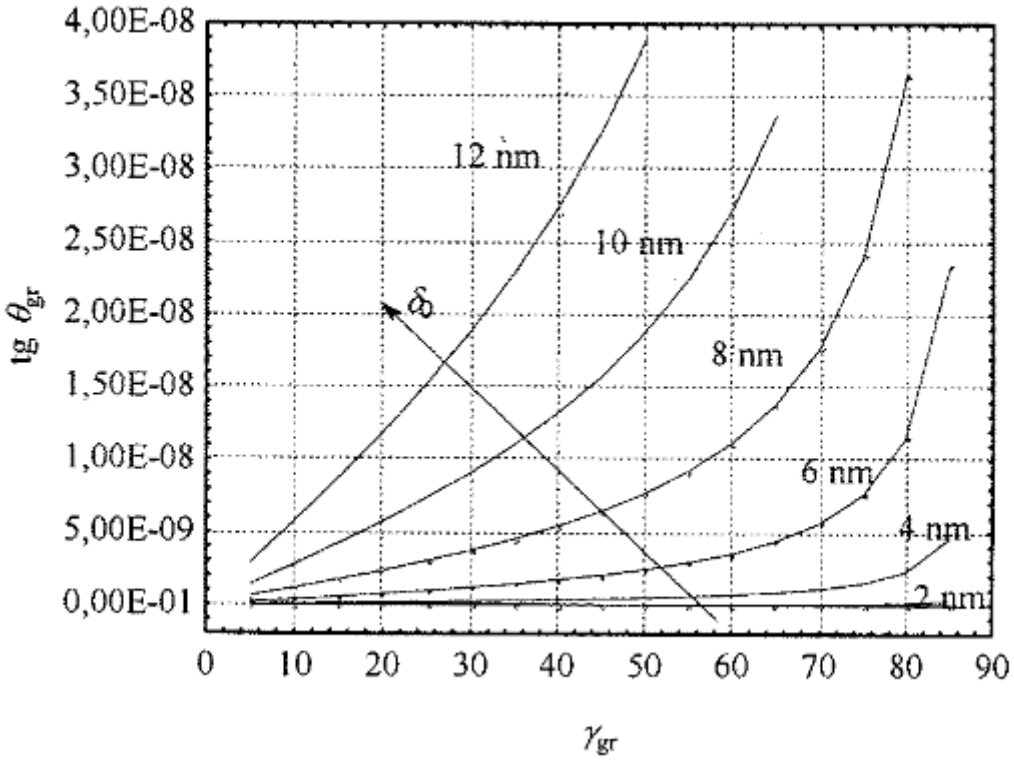

This data of the experimental results must be compared with the next experimental data:

V = 20 µl

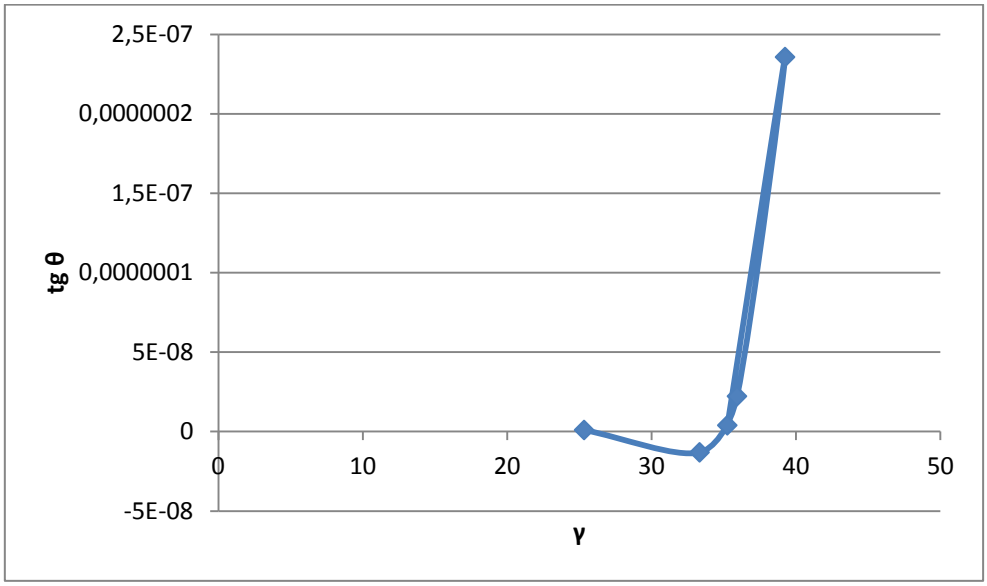

Average values of slope angle of plate with relationship to tg θ.

V (nl)	γaverage (°)	tg θ
5	52,5	-1,11089E-08
10	26,37	1,84269E-08
15	26,19	9,45329E-09
20	35,94	2,46196E-08
25	22,55	2,65703E-09
30	19,05	7,96059E-10
35	15,8	3,37688E-10
40	14,46	-1,03064E-08
45	18,98	4,29255E-10
50	17,52	-1,26908E-08

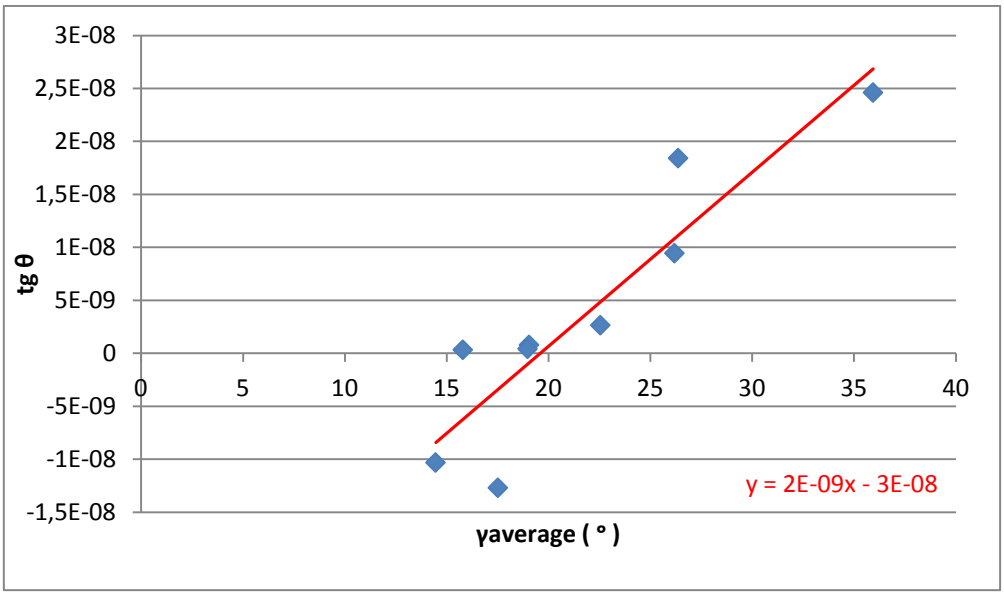

This graph shows that exists a lineal relation between slope angle of plate and tg θ. But the two negative values must be deleted because some error in the measurements can be happened.

Then the next graph, show the correct relation between this parameters:

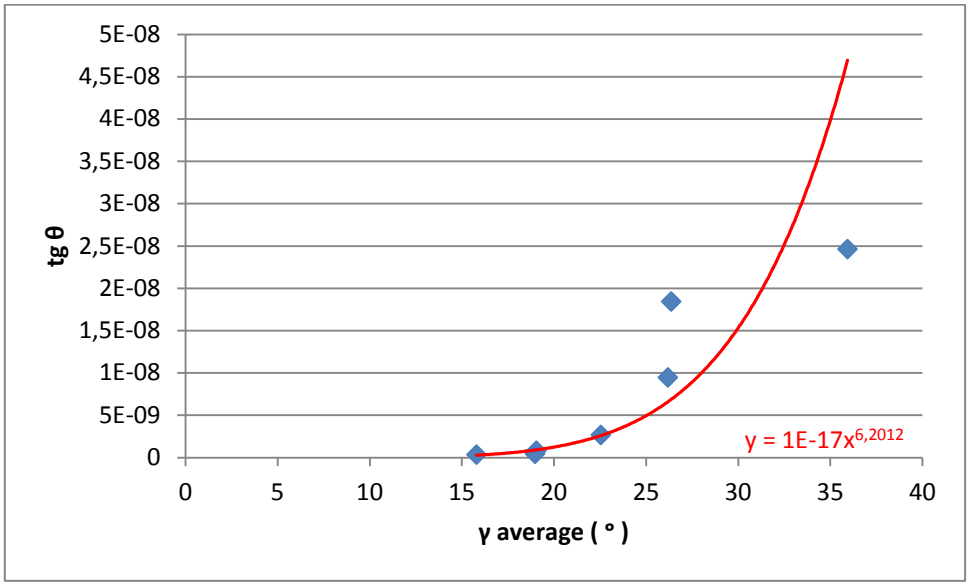

And the next graph shows the relation of volume of droplet between slope angle of plate in different times of measurements.

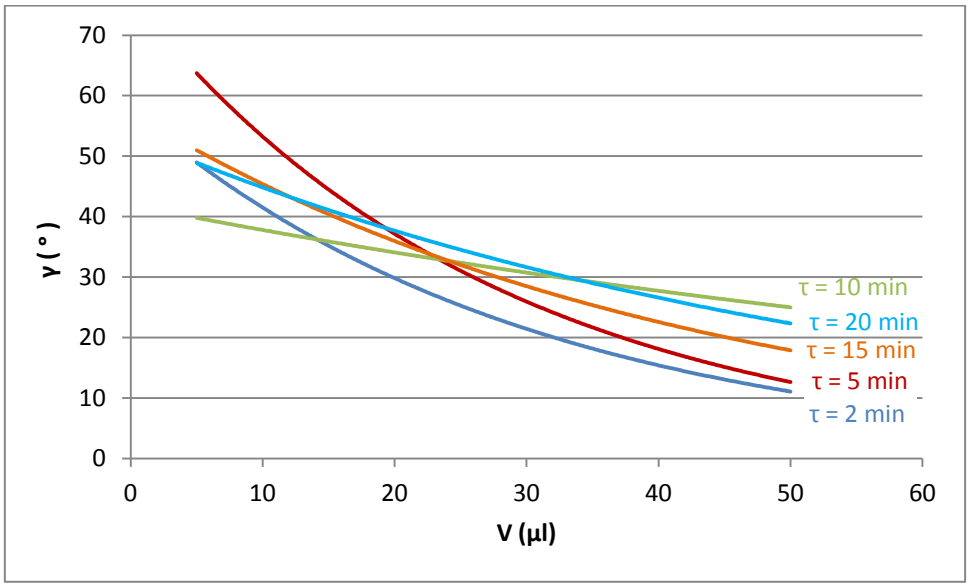

9. Conclusions

Comparing the experimental data with the experimental results by Zapalowicz we can explain the next conclusions about the verification of the model of droplet´s spreading on the solid body surface coated with a water microfilm.

- The values of the dynamic microscopic advanced angle have been estimated with a small range of error.

- The process of evaluated of thickness microfilm by Vladimir S Ajaev for each volume of droplet, allows estimate the dynamic microscopic advanced angle with high grade of verification

- The relationship between the slope angle of plate and dynamic microscopic advanced angle for equals and different values of thickness of microfilm, it is similar.

  For small values of slope angle of plate is almost lineal. For bigger values, the relationship is more difficult of evaluate. The humidity of air and volume of water droplets can be very important in this aspect. On the other hand, the influence of temperature is not important.

- The slope angle oh plate depends directly on the humidity of the air. When the humidity increases, the slope angle of plate decreases.

- The slope angle of plate depends on the temperature of air in according to the experiment. When temperature increases, the slope angle of plate decreases. But the range of temperature is very small (about 2 °C) and this conclusion can be wrong, it is only a supposition.

- The slope angle of plate depends directly on the volume of water droplet. When volume increases, the slope angle of plate decreases.

- The influence of the time in this phenomena it can't be evaluated. More experiments are needed for finding conclusions about this aspect.

10. Bibliography

- Peter C. Wayner, Jr., " Intermolecular forces in phase - change heat transfer: 1998 Kern award review " 1999.
- Karl Stephan, " Influence of dispersion forces on phase equilibria between thin liquid films and their vapour" 2002.
- Vladimir S. Ajaev, " Spreading of thin volatile liquid droplets on uniformly heated surfaces, 2003
- Zbigniew Zapałowicz, " Initial verification of the model of droplets spreading on the solid body surface presence of liquid microfilm" 2003.